QUARTERLY REPORT

April 1, 2024 – June 30, 2024

Kentucky Tobacco Research & Development Center

Martin-Gatton College of Agriculture, Food and Environment

Martin-Gatton
College of Agriculture,
Food and Environment

MEMORANDUM

DATE: July 31, 2024

TO: Kentucky Tobacco Research Board Members
Legislative Research Commission

FROM: Dr. Ling Yuan
Managing Director, KTRDC

SUBJECT: Kentucky Tobacco Research & Development Center
Quarterly Report for April 1, 2024 – June 30, 2024

Enclosed is a copy of the Kentucky Tobacco Research & Development Center's Quarterly Report for April 1, 2024 – June 30, 2024.

If you have any questions, please feel welcome to contact me at (859) 257-5798 or email lyuan3@uky.edu.

Enc.

TABLE OF CONTENTS

EXECUTIVE SUMMARY

Introduction

The legislation (KRS 248.510 - 248.580) which provides funds in support of the research programs at the Kentucky Tobacco Research and Development Center (KTRDC) requires that a quarterly research report be submitted to the Kentucky Tobacco Research Board (KTRB) and the Legislative Research Commission.

The overall reporting plan is:

January 1	-	March 31:	Selected topics
April 1	-	June 30:	Selected topics
July 1	-	September 30:	Selected topics
October 1	-	December 31:	Annual comprehensive report

As required by KRS 248.570, a financial report covering expenditures for the relevant proportion of the July 1, 2023 – June 30, 2024 fiscal year is included in this report.

The news and research publications provided in this quarterly report are a representative selection of the Center's output. For a full description of all KTRDC research and activities please refer to the KTRDC Annual Report.

Quarterly News

- While the emphasis in KTRDC's research work continues to be on harm reduction, there are several other projects.
  - Harm reduction projects in progress for the 2024 season include:
    - Three field and three molecular projects on low alkaloids. These are:
      - A CORESTA collaborative study combining low alkaloid (LA) lines with agronomic practices.
      - A breeding project combining a novel low nicotine gene discovered by the KTRDC field group with the existing LA lines (*nic1 nic2* mutants).
      - An agronomic trial testing the lines mentioned above (novel gene stacked with *nic1 nic2* mutants).
      - A molecular biology study on the metabolic connection between low alkaloid levels and poor leaf quality.
      - Two molecular biology studies on ways to lower nicotine levels.

- Two field and two molecular projects on TSNA (Tobacco-Specific Nitrosamine) reduction. These are:
  - One field and one molecular project on the effect of potassium chloride on TSNAs, and we are coordinating an international CORESTA collaborative study on the topic.
  - One project on TSNAs and green burley. The Council for Burley Tobacco has generously contributed to the funding for this project. In addition to the agronomic and breeding plots on the university farm, two of these lines are being tested on a farm, with the seedlings being produced by the KTRDC field group.
  - The molecular project on nicotine conversion has ended.
- There are two *Artemisia* field projects, where KTRDC is cooperating with UK Pharmacy. *Artemisia annua* (sweet wormwood) is grown for artemisinin, traditionally used as a treatment for malaria, but there is renewed interest in its anti-cancer properties.
- KTRDC is collaborating with the UK Cannabis Center to produce cannabis for clinical behavioral studies. The cannabis plants will be grown in a specially adapted secure growth room. Low delta-9-tetrahydrocannabinol (THC) hemp plants have been successfully grown in the growth room to test the facility. The Drug Enforcement Administration (DEA) will inspect the facility in the next few months.
- Other projects include a black shank CORESTA collaborative trial, and some basic molecular work.

- Activity at the farm involved mainly seedling production and transplanting.
  - Work in April was limited to the care of seedlings in the greenhouse, and servicing and checking equipment for up-coming field operations.
  - May's activities mainly involved transferring seedlings into float trays in a predetermined sequence corresponding to the randomized order of treatments in the field, followed by transplanting.
    - The first transplanting of the tobacco field trials on the university farm was done on May 21, and the last one on May 31.
    - The on-farm green burley was transplanted in Bourbon County on June 1. This tobacco has grown out very well.

    - An on-farm black shank trial was transplanted in Clark County on June 11. At the first count, two weeks after transplanting, signs of disease were already evident.
    - The *Artemisia annua* trials were transplanted on June 13, and drip irrigation was applied the same day.
- The tobacco crop suffered a long hot, dry period, necessitating irrigation. Drip irrigation was started on July 1 for the agronomic trials, and July 9 for the seed field. Regular irrigation was continued until the onset of the rains in late July.
- The March board meeting was held in the KTRDC conference room and by Zoom.
    - Mr. Darrell Varner has been nominated for the vacant member at large position, awaiting approval by the governor.
    - Mr. Hoppy Henton resigned his position as vice chairman and board member representing the Council for Burley Tobacco. He has been replaced on the board as the Council for Burley Tobacco representative by Mr. Al Pedigo. The chairman presented a recognition plaque to Mr. Henton, and thanked him for his years of service. A new vice chairman will be elected at the September board meeting.
    - Dr. Yuan presented the 2024-25 proposed budget and compared it to the current 2023-24 budget. He proposed $20,000 less for the 2024-25 budget. Income projections are lower than last year, continuing the downward trend.
    - Dr. Andy Bailey gave a presentation entitled “Cigar Wrapper Tobacco Research Summary 2019-2023”. He emphasized that the profitability of Connecticut Broadleaf is entirely dependent on the amount of wrapper-grade leaf that can be produced. Based on current budgets, at least 50% of the crop needs to be wrapper grade (at least two wrapper cuts per leaf) to be profitable. The research projects have included nitrogen rate trials, variety trials, curing trials with supplemental heat, fungicide trials, and lower leaf removal trials. In addition, the University of Kentucky is collaborating with the University of Arkansas to evaluate the relationship between frogeye leaf spot disease and ‘greenspot’ of cured leaf, which is one of the major problems seen in CT Broadleaf grown in Kentucky and Tennessee.
- Abstracts have been submitted for the two main tobacco conferences.
    - Abstracts for the CORESTA conference were submitted in late May. Three papers, two reports and one poster from KTRDC have been accepted for the CORESTA congress in October, to be held in Edinburgh, Scotland.

- Abstracts for the TSRC conference were submitted in late May. Five papers and two posters from KTRDC have been accepted for the conference in September, to be held in Atlanta, Georgia. In addition, KTRDC is hosting a reference product workshop where there will be several more presentations. One of the KTRDC graduate students has been awarded the TSRC Scholarship.

- The Center for Tobacco Reference Products (CTRP) proficiency testing (PT) program currently covers the certified reference cigarette, 1R6F, and the certified reference smokeless tobacco products, 1S4, 1S5, 3S1 and 3S3.
  - The current PT rounds are:
    - CIG-2024A – The parameters for this round of testing include the smoking parameters o-Toluidine, 2,6-Dimethylanilin, o-Anisidine, 1-Amino-naphthalene, 2-Aminonaphthalene, 3-Aminobiphenyl, 4-Aminobiphenyl, Total Particulate Matter (TPM), Puff Count, Benzo[α]pyrene (BaP), BaP-Total Particulate Matter (BaP-TPM) and BaP-Puff Count, using the 1R6F reference cigarette as the proficiency test material smoked in both the non-intense and intense smoking regimes. This round of testing opened in January 2024 and the data portal for participants to upload data closed March 2024. The interim report was released for participant review in March 2024 and the final report was released in June 2024.
    - CIG-2024B – The parameters for this round of testing include the smoking parameters Ammonia, Acrylonitrile, Isoprene, Benzene, Toluene, 1,3 Butadiene, Total Particulate Matter, and Puff Count using the 1R6F reference cigarette as the proficiency test material smoked in both the non-intense and the intense smoking regimes. This round of testing opened in March 2024 and the data portal for participants to upload data will close in August 2024.
    - CIG-2024C – The parameters for this round of testing include the smoking parameters Formaldehyde, Acetaldehyde, Acetone, Acrolein, Propionaldehyde, Crotonaldehyde, 2-Butanone, n-Butyraldehyde, and Puff Count using the 1R6F reference cigarette as the proficiency test material smoked in both non-Intense and the Intense smoking regimes. This test also includes the determination of physical properties of the test material, namely: Cigarette Resistance to Draw (pressure drop open), Cigarette Resistance to Draw (pressure drop closed), Filter Pressure Drop (fully encapsulated), Total Ventilation, Filter Ventilation, Tobacco Weight,

Cigarette Weight, Air Permeability, Firmness, Circumference, Cigarette Length, Filter Plug Length, and Tipping Paper Length. This round of testing opened in June 2024. The data portal for participants to upload data is scheduled to close in August 2024.

- Only one of the three Food & Drug Administration (FDA) grants awarded to the University of Kentucky, Center for Tobacco Reference Products (CTRP), to produce and distribute tobacco reference products, is still in effect: the Cigar Tobacco Reference Products (RFA-FD-20-002) grant.
  - The COVID pandemic significantly impacted this project and led to delays in the manufacturing, characterization, and distribution schedule set forth in the grant proposal timeline.
    - Three ISO 17025 accredited laboratories (Labstat, Global and Enthalpy) have completed the characterization process for the large cigar (1RLC) manufactured by ITG Brands (Imperial Tobacco Group). These laboratories have completed the physical measurements and chemical analysis based on the requirements and list of Harmful and Potentially Harmful Constituents (HPHCs) set forth in the grant. The CTRP has finalized the Certificate of Analysis (CoA) and the FDA has reviewed and approved the CoA for distribution to the research community. The CTRP also prepared and submitted to the FDA a Homogeneity Analysis Report for the 1RLC, including six-months of long-term stability analysis data. The 1RLC is listed on the CTRP website and is available for purchase by tobacco research scientists.
    - Two of the three ISO 17025 accredited laboratories (Labstat and Enthalpy) have completed the characterization process for the cigarillo/small cigar (1RSC) manufactured by Swedish Match. These laboratories followed the CTRP protocol for the physical measurements and chemical analysis based on the requirements and list of HPHCs set forth in the grant.
    - Two of the three ISO 17025 accredited laboratories (Labstat and Enthalpy) have completed the characterization process for the filtered cigar (1RFC) manufactured by Scandinavian Tobacco Group (STG).
    - The CTRP was notified by Global that the company was going out of business and would not be able to do the characterization analysis on the 1RSC or the 1RFC. The CTRP began an extensive process of exploring options to contract with an ISO 17025 accredited laboratory to replace

Global as the third analytical laboratory. Additionally, the CTRP was notified on November 27, 2023, that Enthalpy was being acquired by McKinney Specialty Laboratories (MSL) with the transaction scheduled to close prior to year-end. MSL acquired the analytical equipment, retained the personnel of Enthalpy, and the ISO accreditations were transferred to MSL.

- After a lengthy due diligence process, including discussions with commercial laboratories, manufacturers, and other institutions, and in consultation with the FDA, it was decided that the best path forward was to contract with Labstat and MSL to do an additional series of characterization analyses for the 1RSC (cigarillo) and the 1RFC (filtered cigar) following the CTRP protocol for the physical measurements and chemical analysis, based on the requirements and list of HPHCs set forth in the Collaborative Agreement to meet the goals of the grant. Based on this option, the CTRP will be obtaining four datasets by using both laboratories (Labstat and Enthalpy/MSL) to test both the 1RSC and 1RFC, which would produce sufficient data to establish a true data range for the analytes, thereby creating a better understanding of the variation of these cigar analytes and physical parameters.
- Due to budget constraints and the additional characterization analysis agreed on, the CTRP requested additional funding for the cigar project in the amount of $484,609 to successfully complete the specific objectives set forth in the Collaborative Agreement. This additional funding request was granted by the FDA and was awarded on February 10, 2024. The additional funding is being used to fully complete the characterization of the reference cigarillo (1RSC) and filtered cigar (1RFC) by contracting with two ISO 17025 accredited laboratories (Labstat and MSL) to conduct an additional series of characterization analyses for both reference cigar products following the CTRP protocol for the physical measurements and chemical analysis based on the requirements and list of HPHCs set forth in the Collaborative Agreement ($334,213) and for the overhead expenses required by UK federal contracting guidelines ($150,396).
- The main achievements for this reporting period include: (1) receipt of datasets from Labstat and MSL for the cigarillo (1RSC) reference cigar; (2) characterization analysis, audit, and statistical analysis for the 1RSC, including drafting preliminary CoA; (3) receipt of the dataset from Labstat for the filtered cigar (1RFC); (4) continued progress on the analysis of the

commercial cigars; (5) continued progress on the long-term stability studies on the previously manufactured non-certified CTRP reference cigars and the new reference cigars: 1RLC, 1RSC and 1RFC; and (6) continued progress on research projects.

- Four datasets for the characterization of the cigarillo/small cigar (1RSC) manufactured by Swedish Match have been completed. The laboratories have completed the physical measurements and chemical analysis based on the requirements and list of HPHCs set forth in the Collaborative Agreement. Characterization analyses of the cigarillo (1RSC) reference product were the last analyses completed.
- The CTRP has drafted a preliminary CoA and will input the analytical values once the characterization analysis, audit, and statistical analysis and review are complete, which is expected to be in July 2024.
- Three of the ISO 17025 accredited laboratories have completed the characterization process for the filtered cigar (1RFC) manufactured by Scandinavian Tobacco Group (STG). These laboratories have completed the physical measurements and chemical analysis based on the requirements and list of HPHCs set forth in the Collaborative Agreement. MSL indicated that the laboratory would complete the analysis of the 1RFC mid-July 2024.
- The CTRP analytical laboratory has continued research on the commercial cigar products according to the research plans presented to the FDA.
- The CTRP analytical laboratory continues the long-term stability studies on the certified CTRP reference cigars: 1RLC, 1RSC and 1RFC.
- Our research scientists continue to make progress on their tobacco science research projects, including microbial method development, analytical method development, metal analysis, and toxicological research on reference and commercial cigar products.

I would like to thank Mr. Matthew Craft and Dr. Ruth McNees for their help with some sections of this report.

The KTRDC Quarterly Reports include copies and brief summaries of work published by KTRDC scientists and scientists partly funded by KTRDC. I would like to thank Ms. Huihua Ji and Dr. Sitakanta Pattanaik for their help with writing the summaries.

Summary of Selected Research Topics

Report #1 *"Long-term storage study of the certified 1R6F reference cigarette."*

Huihua Ji, Laura Fenton, Siqi Guan and Ying Wu

This paper deals with the study of the stability of constituents in the reference cigarette 1R6F. This research is important because reference tobacco products are crucially important to report, compare, and interpret constituent levels in tobacco products, and stability is a crucial factor for reference products used over time: however, there is little published data to demonstrate the stability of the 1R6F cigarette. The major finding was that no significant differences in the major constituents were detected after storage of the 1R6F cigarette at -20°C for three years. The findings of this research demonstrated that the 1R6F reference cigarette meets stability requirements, and is a good reference product.

The first certified reference cigarette, 1R6F, was produced by the Center for Tobacco Reference Products at the University of Kentucky in 2015 and certified in 2016. 1R6F reference cigarettes have been stored at -20˚C since they were manufactured. 1R6F has been widely used as a control cigarette or a monitor for non-clinical investigational purposes in tobacco product analysis and scientific research. However, there is little published data to demonstrate the stability of the 1R6F cigarette. In this paper, we report the results of a long-term storage study of the 1R6F cigarette. Data are reported for both mainstream smoke and tobacco filler. 1R6F cigarettes were stored under different conditions (room temperature, refrigerator (4°C), and freezer (-20°C)) for three years, from April 2017. The constituents in the cigarette tobacco filler (oven volatiles, nicotine, NNN, and NNK) and the mainstream smoke (nicotine, NNN, NNK, B[α]P, CO, and TPM) were analyzed. Some physical parameters (resistance to draw and ventilation) were also measured. Analysis of our data showed that no significant differences in these major constituents were detected after storage of the 1R6F cigarette at -20°C for three years.

Report #2 *"Partial desensitization of MYC2 transcription factor alters the interaction with jasmonate signaling components and affects specialized metabolism*."

Xin Hou, Sanjay Singh, Joshua Werkman, Yongliang Liu, Xia Wu, Barunava Patra, Xueyi Sui, Ruiqing Lyu, Bingwa Wang, Xiaoyu Liu, Wei Ma, Sitakanta Pattanaik and Ling Yuan

This paper describes engineering transcription factors to manipulate metabolic pathways (including nicotine synthesis) in plants. This work is important because, using tobacco as a model, it demonstrated that engineered or mutant transcription factors can be used to manipulate the nicotine pathway. The major finding was that overexpression of a mutant MYC2 alters nicotine pathway gene expression and nicotine accumulation. This finding is of great interest because this approach can be used to increase nicotine (for use in e-cigarettes and nicotine pouches) or possibly to decrease nicotine (to meet possible regulatory targets).

Transcription factors contain multiple distinct domains that are involved in DNA binding, protein-protein interaction and transcriptional activation or repression. The modular nature of transcription factors has led to the idea that specific modules (domains) of transcription factors can be redesigned to regulate desired gene(s) through protein engineering. The ability to generate designer transcription factors has the potential to aid in our understanding of gene regulation and is of biotechnological interest. The basic helix-loop-helix (bHLH) transcription factor MYC2 is a regulator of many specialized metabolites such as the therapeutic compounds paclitaxel in Taxus, terpenoid indole alkaloids in periwinkle and artemisinin in Artemisia. MYC2 is also a key regulator of nicotine biosynthesis in tobacco. MYC2 contains multiple distinct domains such as the amino-terminus JAZ interaction domain (JID), transactivation domain and DNA binding domain. The JID domain of MYC2 is important for interaction with jasmonate ZIM domain (JAZ) proteins, which are repressors of nicotine biosynthesis. A previous study has shown that mutation of a conserved aspartic acid to asparagine in the JID of Arabidopsis MYC2 inhibits its interaction with JAZ proteins. The conserved regulatory roles of MYC2 across plant species prompted us to further explore the potential effects of mutations in MYC2 JID in the regulation of specialized metabolism, using tobacco as a model. We demonstrated that the mutation of the conserved aspartic acid in the JID of MYC2 affects its interaction with tobacco JAZ proteins and alters its activity on key nicotine pathway gene promoters. Additionally, overexpression of mutant MYC2 in tobacco hairy roots alters nicotine pathway gene expression and nicotine accumulation. Regulation of many plant specialized metabolic pathways are well conserved across the species, and our work provides an innovative approach to engineering metabolic pathways to increase the production of medicinal compounds by targeting the ability of a transcription factor to interact

with co-regulators. This approach could be used to increase nicotine accumulation for nicotine extraction, for use in e-cigarettes and nicotine pouches. It is also possible that this approach could be modified to reduce nicotine, to meet possible regulatory targets.

Chemical Research in Toxicology

pubs.acs.org/crt

Article

Long-Term Storage Study of the Certified 1R6F Reference Cigarette

Huihua Ji,* Laura Fenton, Stacey Slone, Siqi Guan, and Ying Wu

Cite This: *Chem. Res. Toxicol.* 2023, 36, 685−690

Read Online

ACCESS | Metrics & More | Article Recommendations

ABSTRACT: The first certified reference cigarette, 1R6F, was produced by the Center for Tobacco Reference Products at the University of Kentucky in 2015 and certified in 2016. 1R6F reference cigarettes have been stored at −20 °C since they were manufactured. 1R6F has been widely used as a control cigarette or a monitor for nonclinical investigational purposes in tobacco product analysis and scientific research. However, there is little published data to demonstrate the stability of the 1R6F cigarette. In this paper, we report the results of a long-term storage study of the 1R6F cigarette tobacco filler and the resulting mainstream smoke. 1R6F cigarettes were stored under different conditions (room temperature, refrigerator (4 °C), and freezer (−20 °C)) for 3 years since April 2017. The constituents in the cigarette tobacco filler (oven volatiles, nicotine, *N*′-nitrosornicotine (NNN), and 4-(methylnitrosamino)-1-(3-pyridyl)-1-butanone (NNK)) and the mainstream smoke (nicotine, NNN, NNK, benzo[α]pyrene, carbon monoxide, total particulate matter) were analyzed. Some physical parameters (resistance to draw and ventilation) were also measured. Analysis of our data showed that no significant differences in these major constituents were detected after storage of the 1R6F cigarette at −20 °C for 3 years.

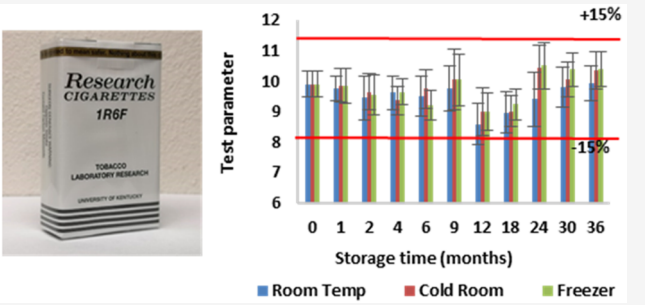

1. INTRODUCTION

It is well-known that cigarette smoking is harmful to many body organs and causes negative human health issues such as cancers, heart disease, stroke, lung disease, and diabetes.[1] Approximately 14% of adults aged 18 years or older (an estimated 34.2 million) were cigarette smokers in the United States in 2018.[2] In March 2012, the US Food and Drug Administration (FDA) established a list of harmful and potentially harmful constituents (HPHCs) in tobacco products and tobacco smoke.[3] In August 2016, the FDA issued a final rule to regulate all tobacco products that included cigarettes, cigarette tobacco, cigars, roll-your-own tobacco, smokeless tobacco products, and any other tobacco products. The FDA requires tobacco companies to report the levels of HPHCs found in their tobacco products and tobacco smoke. In addition, any new tobacco products need to be submitted as a premarket tobacco product application (PMTA) to the FDA before the new tobacco product can be marketed.[4] The use of reference materials is essential to PMTA. Reference tobacco products are crucially important to report, compare, and interpret the levels of HPHCs in tobacco products. The reporting or publication of data might be misinterpreted without the inclusion of certified reference materials in the communication. Currently, more and more studies have documented the application of reference cigarettes in their research.[5−10]

Based on the International Organization for Standardization (ISO) Guide, "Reference material is the material that is sufficiently homogeneous and stable with respect to one or more specified properties, which has been established to be fit for its intended use in a measurement process".[11] Stability is a crucial factor for reference material. The University of Kentucky Center for Tobacco Reference Products (CTRP) has provided reference cigarettes for almost 50 years. These reference cigarettes are widely used as control samples for nonclinical investigational purposes of tobacco research including analytical method development and modified risk tobacco product development. In 2014, CTRP obtained a service agreement with the FDA to produce a certified reference cigarette. The first certified reference cigarette, 1R6F, was manufactured in March 2015. The 1R6F reference cigarettes were manufactured at one time and over 50 million cigarettes were produced, which is enough to last for many years. One crucial property of reference material that is intended to be supplied for many years is its stability in long-term storage. However, there are presently no data showing the stability of 1R6F cigarettes in long-term storage. In this paper, 1R6F cigarette tobacco filler and the resulting mainstream cigarette smoke (including some key constituents in the

Received: January 5, 2023
Published: March 16, 2023

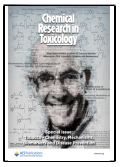

HPHCs list) were analyzed to evaluate the stability of the reference material under long-term storage.

In our study, the constituents in cigarette tobacco filler (oven volatiles, nicotine, and tobacco-specific N-nitrosamines (TSNAs) including *N*′-nitrosornicotine (NNN) and 4-(methylnitrosamino)-1-(3-pyridyl)-1-butanone (NNK)) and the constituents in mainstream cigarette smoke (nicotine, NNN, NNK, benzo[α]pyrene (B[α]P), carbon monoxide (CO), total particulate matter (TPM)) and puff counts were analyzed at different storage times and storage conditions (room temperature (22 °C), refrigerator (4 °C), and freezer (−20 °C)). Physical parameters including resistance to draw and ventilation were also measured. Our results showed that there were no significant differences in these major constituents of 1R6F cigarettes that had been stored at −20 °C for three years.

2. EXPERIMENTAL SECTION

2.1. Samples. The 1R6F certified reference cigarettes were purchased from the CTRP at the University of Kentucky. 1R6F, the first certified reference cigarette, was designed to be representative of American market blended tobacco cigarettes. The 1R6F was produced only for research purposes and is not intended for human consumption.

The reference material (RT1−1R6F ground filler) was purchased from the CTRP at the University of Kentucky.

2.2. Reagents. Standard nicotine, B[α]P, and the internal standard B[α]P-d_{12} were purchased from Sigma-Aldrich (St. Louis, MO). Standards for TSNAs (NNN and NNK) and *N*-nitroso-di-*n*-hexylamine (NDHA) were purchased from Toronto Research Chemicals (Ontario, Canada). Dibasic sodium phosphate (Na_2HPO_4), sodium hydroxide (NaOH), and citric acid were purchased from Sigma-Aldrich (St. Louis, MO). Quinoline, LC-MS grade acetonitrile, HPLC grade methyl tertiary-butyl ether (MTBE), HPLC grade methanol, 99.8% toluene, HPLC grade methylene chloride, and LC-MS grade water were purchased from Fisher Scientific (Fairlawn, NJ, USA).

2.3. Sample Preparation. Two cases of 1R6F certified reference cigarettes were purchased from the CTRP at the University of Kentucky in April 2017. The samples were divided into three groups when they were received from the CTRP. Each group of cigarettes was stored in two Ziploc-sealed plastic bags and stored under different conditions. One group of cigarettes was stored at room temperature (~22 °C), the second group of cigarettes was stored in a refrigerator (4 °C), and the third group of cigarettes was stored in a frost-free freezer (−20 °C). After each storage interval (0, 1, 2, 4, 6, 9, 12, 18, 24, 30, and 36 months), a subsample of cigarettes from each group was removed from the storage place and conditioned for cigarette smoking and tobacco filler analysis. Before the 1R6F cigarettes were analyzed, they were transferred stepwise from these storage conditions until they reached room temperature. Cigarettes stored at −20 °C were transferred to 4 °C for 24 h then room temperature for at least 2 h or until they had reached equilibrium; cigarettes stored at 4 °C were transferred to room temperature for at least 2 h or until they had reached equilibrium. The reference cigarettes from the three different storage conditions were then conditioned for 48 h at 22 °C and 60% relative humidity according to ISO 3402:1999,[12] prior to the analysis of the tobacco filler (except oven volatiles) and the smoking of the cigarettes.

2.4. Smoking Cigarettes and 1R6F Filler Analysis. The sampled cigarettes for smoking were conditioned for 48 h at 22 °C and 60% relative humidity prior to smoking according to ISO 3402:1999. 1R6F cigarettes were smoked under ISO smoking conditions and the standard non-intense smoking regime ISO 3308:2012 (35 mL puff volume, 2 s puff duration, and 60 s puff frequency) using a Cerulean SM450 linear smoking machine (United Kingdom).[13,14] The smoke condensate was collected on a Cambridge filter pad. The mainstream smoke analyses included the measurement of nicotine, NNN, NNK, B[α]P, CO levels, TPM, and puff counts. Each data point for CO, TPM, and puff count was a mean value from 25 replicates that was the combined data from all smoke determinations for each constituent, while each data point for nicotine, NNN, NNK, and B[α]P was a mean value from five replicates. Each replicate is the mean value of five cigarettes smoked in a continuous sequence in the same port.

1R6F filler analyses included oven volatiles, nicotine, NNN, and NNK. The tobacco filler was removed from the cigarette by cutting the paper of the cigarette. The filler from 15 cigarettes was combined and well mixed to use for chemical analysis. The oven volatiles were measured with three replicates, and nicotine, NNN, and NNK in the filler were analyzed with two replicates. Physical parameters (resistance to draw and ventilation) were also measured.

2.5. Constituents Analysis. Alkaloid levels were measured with a gas chromatography-flame ionization detector using a protocol developed by the Kentucky Tobacco Research and Development Center at the University of Kentucky. The samples were extracted with NaOH and MTBE. A PerkinElmer Auto System XL GC with a backflush system fitted with a Zebron capillary GC ZB-5 column (30 m × 0.53 mm, 1.50 μm film thickness from Phenomenex Inc.) was coupled with FID for alkaloid determinations. The initial column temperature of 200 °C was increased to 230 °C at 20 °C/min and held for 1 min. The temperatures of the injector and detector were 250 and 275 °C, respectively.

TSNAs were measured with a gas chromatography-thermal energy analyzer using a protocol established by a collaborative study under the guidance of the Tobacco Science Research Conference Analytical Methods Committee. The samples were extracted with methylene chloride containing NDHA as an internal standard. An Ellutia 200 series GC with an 815 TEA detector (Witchford, United Kingdom) was equipped with a DB-5 GC column (30 m × 0.53 mm, 1.50 μm film thickness from Agilent J&W) for analysis. The initial column temperature was 125 °C for 30 s, was increased to 220 °C at 6 °C/min for 2 min and then to 280 °C at 20 °C/min, and held for 10 min. The temperatures of the injector, the pyrolizer of the TEA, and the interface oven were 225 °C, 500 °C, and 280 °C, respectively.

B[α]P was measured using the method adapted from the Cooperation Centre for Scientific Research Relative to Tobacco recommended method − CRM 58.[15] An Agilent 7890B GC system (Santa Clara, CA) was coupled with an Agilent 7000C Triple Quad mass spectrometer. Chromatography was performed on a DB-17 GC capillary column (0.25 μm film, 0.25 mm × 30 m, Agilent Technologies). The column temperature was initially held at 200 °C for 1 min, after which it was programmed to increase to 280 °C at 25 °C/min, then from 280 to 320 °C at a rate of 40 °C/min and held there for 5.5 min. Helium was the carrier gas. The inlet and MS source temperatures were maintained at 300 and 250 °C, respectively. The injection volume was 1 μL in the pulsed splitless mode. Agilent 7000C Triple Quad mass spectrometer was operated in an electron ionization source with single ion monitoring mode.

Considering the possibility of the variation from the analytical procedure, the reference material (RT1- 1R6F ground filler) as a control sample was analyzed for these parameters at each time period. The data was compiled from in-house data collection and also compared to the 1R6F ground filler reference material data sheet.[16]

2.6. Physical Parameter Measurements. The physical parameters resistance to draw, filter pressure drop, filter region ventilation (Vf), and overall ventilation (Vo) were measured using an OMI-FLEX test station from Borgwaldt-Hauni GmbH (Hamburg, Germany).

2.7. Statistical Methods. The mean and standard deviation for each analyte were calculated for each condition at each time point. These summary statistics were visually compared with a ±15% confidence band. In addition, simple linear models, $y_i = \beta_0 + \beta_1 Month_i + \varepsilon$, were run for each analyte and condition on the mean values at each time point to get estimates of the β_1. The goal is for the estimated linear equation to fit within the ±15% confidence band over the 36-month study period, and the value of δ for each analyte was

https://doi.org/10.1021/acs.chemrestox.3c00004
Chem. Res. Toxicol. 2023, 36, 685−690

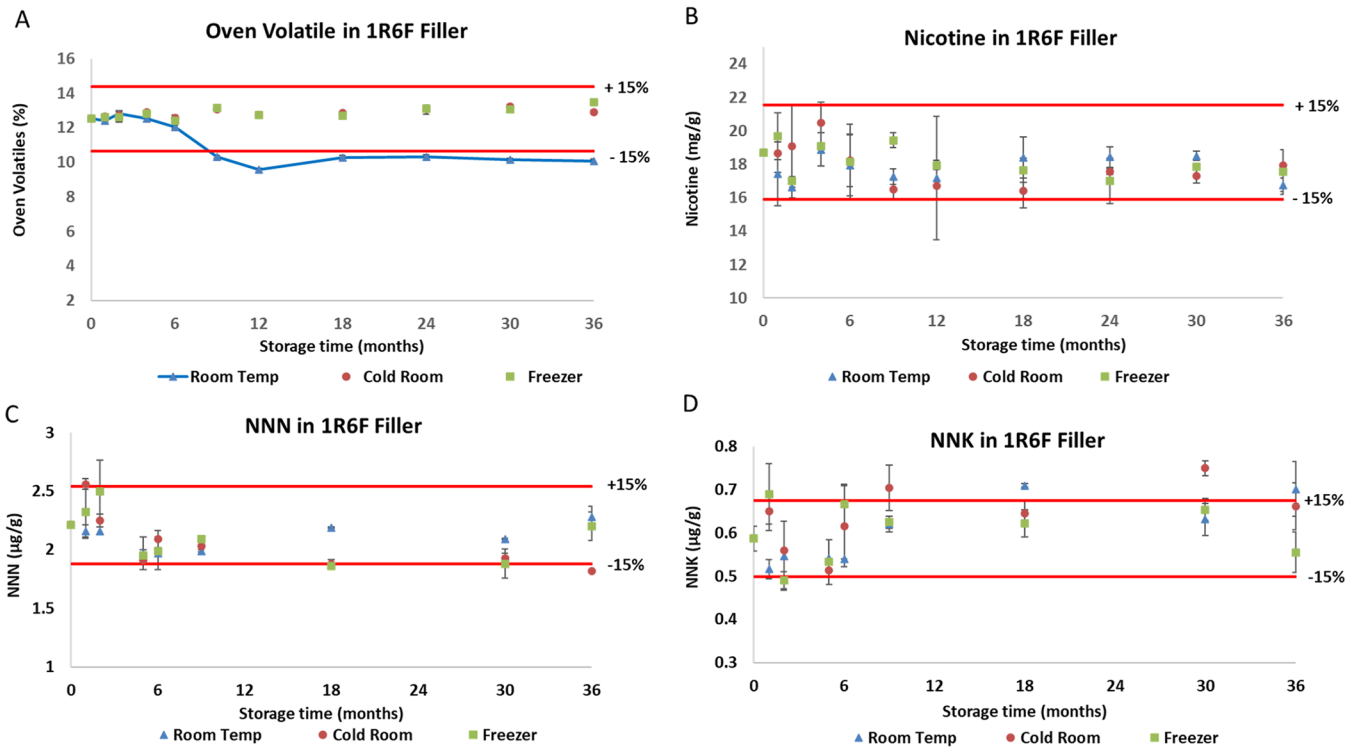

Figure 1. Levels of oven volatiles, nicotine, NNN, and NNK in 1R6F filler tobacco.

calculated using the bound. Equivalence tests were then performed using the 95% confidence interval of the β_1.[17]

3. RESULTS AND DISCUSSION

Typically, to evaluate the stability of an analyte during storage, the approach can be either to compare the stored samples to corresponding freshly prepared samples side-by-side or to compare the values from the stored samples to a reference value. The latter method gives a direct estimate and avoids errors from pre-analytical manipulations, such as the spiking process.[18] The reference value can be either the theoretical value or the value determined at the initial time (t = 0 value) before storage in the experiment. The initial time data (t = 0 value) was used as the reference value in this study. The 1R6F certificate of analysis (COA) value and uncertainty were also considered.[19]

The constituents in cigarette tobacco filler (oven volatiles, nicotine, NNN, and NNK) and the mainstream cigarette smoke (nicotine, NNN, NNK, B[α]P, CO, and TPM) and puff counts were analyzed for the different storage times and storage conditions (room temperature, 4 °C, and −20 °C). Resistance to draw and ventilation were also measured. Nicotine, B[α]P, NNN, and NNK are on the FDA list of HPHCs. Nicotine, a highly addictive chemical, is the most significant alkaloid in tobacco products.[20] TSNAs, especially NNN and NNK, are well-known carcinogens present in tobacco products.[21] NNN and NNK have shown carcinogenicity in animals and potential carcinogenicity in humans.[22] B[α]P, formed during the incomplete combustion of organic matter, has carcinogenic activity because it can form an adduct with deoxyguanosine to covalently modify DNA.[23]

3.1. 1R6F Cigarette Tobacco Filler Results. The data for oven volatiles, nicotine, NNN, and NNK levels in 1R6F tobacco filler that was stored at room temperature, 4 °C, and −20 °C for 3 years are shown in Figure 1. The oven volatiles were measured before the cigarettes were conditioned. The data indicate that the oven volatiles showed a significant change in 1R6F cigarettes that were stored at ambient room temperature, but the volatiles were stable at 4 °C and −20 °C storage conditions (Figure 1A). When 1R6F cigarettes were stored at ambient room temperature, the oven volatiles were decreased by ∼24% after 1 year of storage and then slightly increased in the later testing dates. There are four main factors affecting the evaporation of liquid: temperature, the surface area occupied by the liquid, humidity of the surroundings, and air circulation or wind speed.[24,25] In our study, the products have the same surface area and similar air circulation in the storage area. Therefore, the humidity of the surroundings and temperature are the two main factors affecting evaporation in our study. The relative humidity in the building ranges from 20% to 75% during the year. In the wintertime, the relative humidity in the laboratory is very low. The lower humidity and higher temperature cause more moisture loss in the cigarettes. When the 1R6F cigarettes were stored at 4 °C and −20 °C, the relative humidity range was much narrower (55%−70%) compared to room temperature. The lower temperatures (of 4 °C and −20 °C) result in lower kinetic energy of the individual water molecules, hence more difficult for them to overcome the hydrogen bonding and escape into the atmosphere as water vapor. Consequently, the lower kinetic energy makes the molecule difficult to evaporate.[24,25]

The analyses of nicotine, NNN, and NNK in tobacco filler were performed after the 1R6F cigarettes were conditioned at 22 °C and 60% relative humidity for at least 48 h. The moisture content was consistent with ∼12%−13% after the cigarettes were conditioned. Therefore, the moisture variation at room temperature did not affect the results of the chemical analyses. To evaluate the stability of 1R6F in long-term storage, the concentrations of each analyte determined at the different storage conditions were compared to their initial time

https://doi.org/10.1021/acs.chemrestox.3c00004
Chem. Res. Toxicol. 2023, 36, 685−690

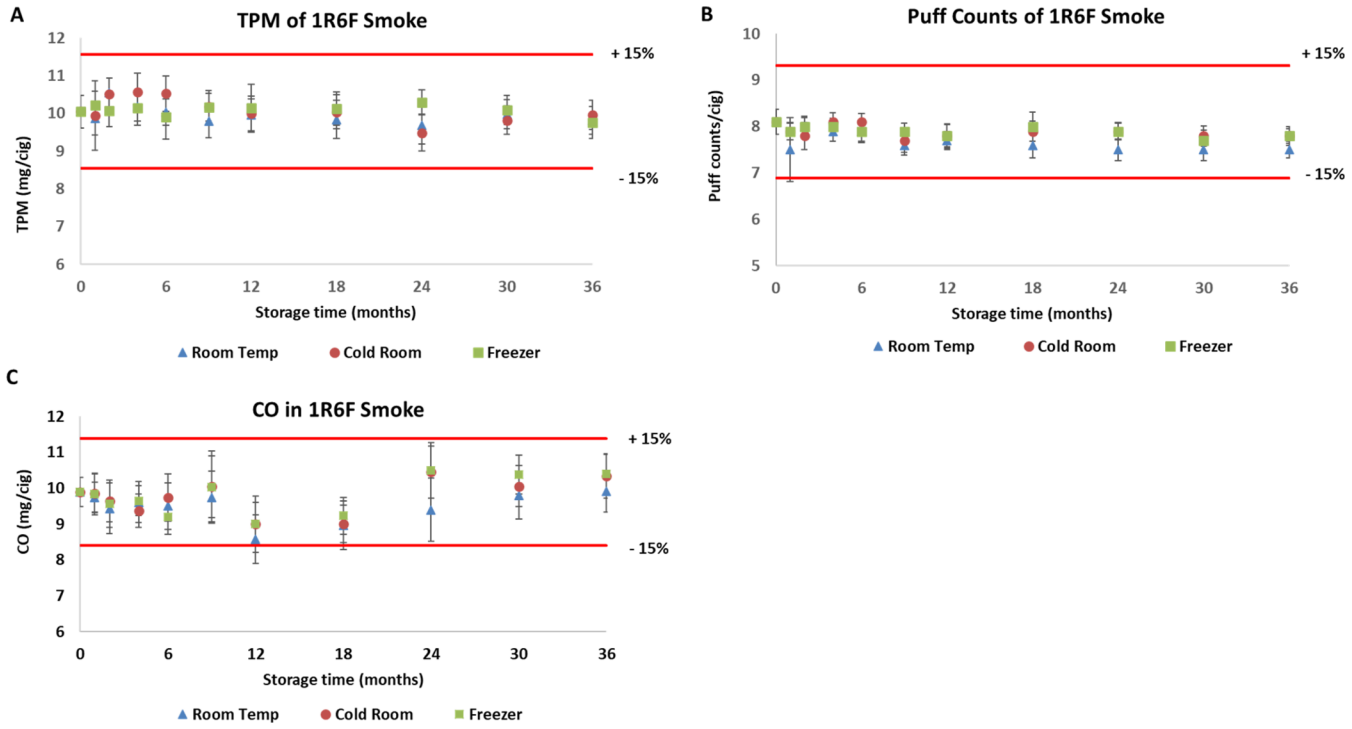

Figure 2. CO level, TPM, and puff counts in the mainstream smoke of 1R6F cigarettes.

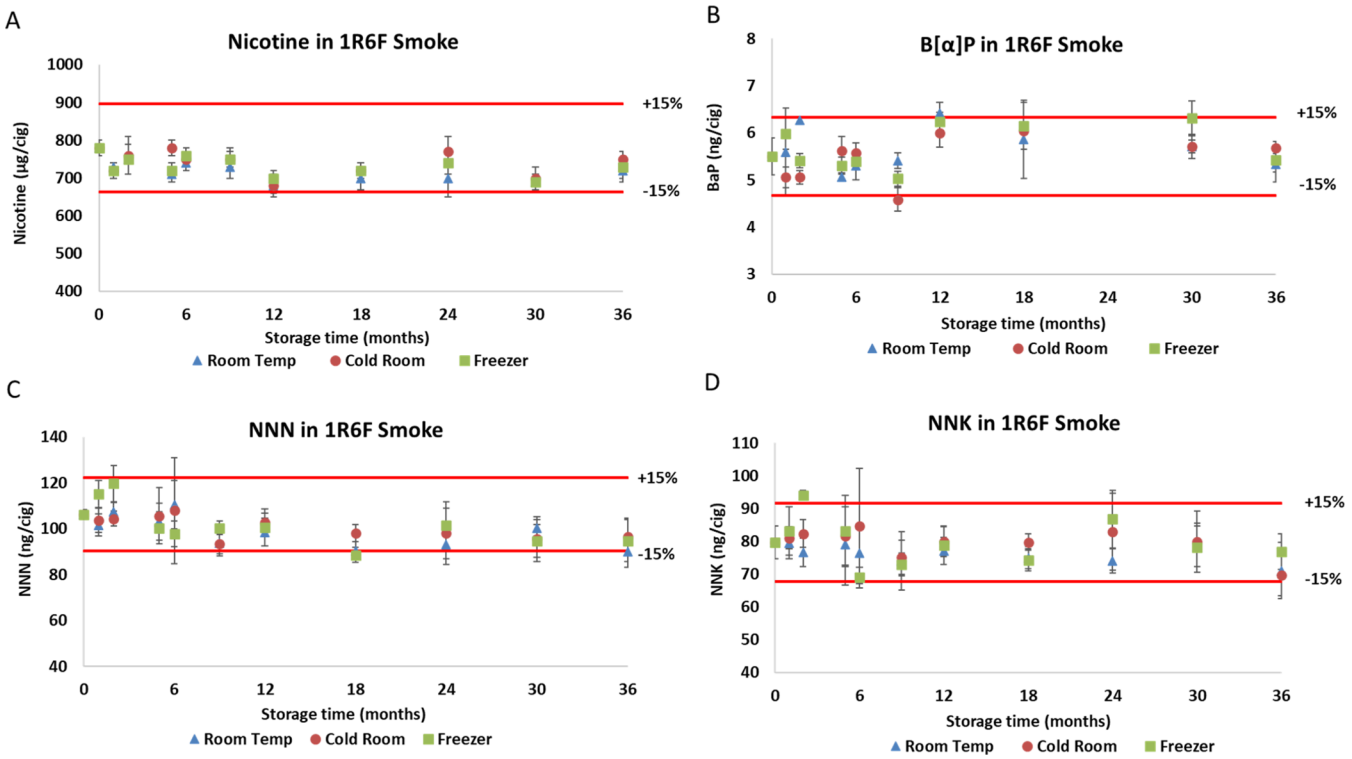

Figure 3. Nicotine, B[α]P, NNN, and NNK levels in the mainstream smoke of 1R6F cigarettes.

value (t = 0). Many factors can affect the amounts of the various analytes detected during storage. The "practical" criteria for the evaluated 1R6F storage study data need to make allowances for both the precision of the analytical method and the natural properties of the tobacco products. Variability in some 1R6F constituents is to be expected because 1R6F is an agricultural product and there is some variability in the raw materials. Also, the relative precision in different analytical methods is different. In general, the value of 15% is commonly recommended as the acceptance criteria for the precision of the analytical method validation.[18,26−28] A sample would be considered unstable if the difference between the values of the stored samples and the reference value is greater than the variation in the precision of the analytical

https://doi.org/10.1021/acs.chemrestox.3c00004
Chem. Res. Toxicol. 2023, 36, 685−690

Table 1. Physical Parameters of 1R6F Cigarettes Stored at −20°C[a]

months	Resistance to draw (mmWg)	Filter pressure drop (mmWg)	Vf (%)	Vo (%)
COA	107 ± 4	137 ± 4	NA	33 ± 6
0	102.00 ± 14.84	141.90 ± 4.76	37.22 ± 9.04	39.63 ± 7.33
1	93.30 ± 19.49	138.10 ± 7.18	41.94 ± 11.68	43.81 ± 8.81
2	101.95 ± 8.80	139.45 ± 5.00	37.29 ± 5.54	40.76 ± 4.09
6	101.35 ± 7.44	135.95 ± 6.75	36.04 ± 3.27	39.19 ± 2.40
9	104.90 ± 4.97	137.80 ± 6.00	34.37 ± 2.02	38.32 ± 2.06
12	107.00 ± 3.81	140.00 ± 4.79	34.14 ± 2.13	38.02 ± 2.09
18	106.15 ± 4.82	139.95 ± 5.75	34.61 ± 1.92	38.91 ± 1.74
24	106.85 ± 3.77	140.35 ± 4.30	NA	NA
30	104.70 ± 4.05	137.40 ± 4.89	33.80 ± 1.54	37.33 ± 1.64
36	106.40 ± 3.73	138.90 ± 4.22	33.60 ± 2.25	37.30 ± 2.14

[a]Vf, filter region ventilation. Vo, overall ventilation. NA, not available.

method.[26] Hence, a 15% evaluation criterion was used to evaluate the stability of 1R6F cigarettes. Most of the results for nicotine, NNN, and NNK in 1R6F cigarette filler fit within the 15% range in the long term storage study (Figure 1B−D). This indicates that nicotine, NNN, and NNK in 1R6F cigarette fillers are stable when stored at room temperature, 4 °C, and −20 °C for 3 years.

3.2. 1R6F Mainstream Smoke Results. The mainstream smoke analysis data (nicotine, NNN, NNK, B[α]P, CO, TPM, and puff counts) of 1R6F cigarettes that were stored at room temperature, 4 °C, and −20 °C for 3 years are shown in Figures 2 and 3. The data of nicotine, NNN, NNK, B[α]P, CO, TPM, and puff counts in the mainstream smoke fit in the 15% range. All these results indicated that there were no significant changes for puff counts, CO, TPM, nicotine, NNN, NNK, and B[α]P in the mainstream smoke of cigarettes stored under room temperature, 4 °C, and −20 °C conditions for 3 years.

3.3. Equivalence Testing. For the filler analyses, equivalence testing supported the consistency of nicotine, while NNK and NNN did not quite reach significance with p's < 0.10. Within the mainstream smoke analyses, the consistency of all of the analytes with the exception of NNN was supported by equivalence testing. While NNN is influenced by the unexpectedly lower result at 18 months, the p-value for the equivalence test is relatively close with $p < 0.11$.

3.4. Physical Parameters. Data for the physical parameters (resistance to draw, filter pressure drop, Vf, and Vo) of the 1R6F cigarettes stored at −20 °C are presented in Table 1. Data for each parameter were the mean of 20 individual cigarettes. The physical parameter data for 1R6F cigarettes stored at room temperature and 4 °C are very similar to cigarettes stored at −20 °C (data are not shown). This suggests that there were no significant changes in the physical parameters of 1R6F cigarettes during the storage period.

3.5. Small Volatile Compounds. The stability of small volatile compounds, such as carbonyl compounds, was not determined in the current study. A project including the stability test for these compounds is ongoing. Nevertheless, a study reported in the literature demonstrated that these small volatile compounds in tobacco products are not stable when stored at room temperature and 4 °C.[29] Therefore, we recommend that the best temperature for long-term storage of the 1R6F certified reference cigarette is −20 °C.

4. CONCLUSION

The certified 1R6F reference cigarettes have been stored at −20 °C since they were manufactured in 2015 and certified in 2016. The results for the contents of oven volatiles, nicotine, NNN, and NNK in the 1R6F cigarette filler are comparable after storage at 4 °C and −20° for 3 years. However, the oven volatiles decreased significantly when the 1R6F cigarettes were stored at room temperature. There were no significant changes in puff counts, CO, TPM, nicotine, B[α]P, NNN, and NNK in the mainstream smoke of 1R6F cigarettes stored at room temperature, 4 °C, and −20 °C. Our experimental data demonstrated that 1R6F cigarettes are stable for the above-selected constituents when stored at 4 °C and −20 °C for 3 years. Overall, we recommend keeping the certified reference cigarettes at −20 °C for long-term storage. This is the first systematic comparison of the long-term storage stability of the reference cigarette tobacco filler as well as the constituents in the 1R6F cigarette smoke for three storage temperatures: room temperature, refrigerator (4 °C), and freezer (−20 °C). The methodology used in this paper can be applied in the future to other reference cigarettes.

AUTHOR INFORMATION

Corresponding Author

Huihua Ji − *Kentucky Tobacco Research and Development Center, University of Kentucky, Lexington, Kentucky 40546, United States;* orcid.org/0000-0001-7528-1036; Phone: +1-859-2180803; Email: hji4@uky.edu

Authors

Laura Fenton − *Kentucky Tobacco Research and Development Center, University of Kentucky, Lexington, Kentucky 40546, United States*

Stacey Slone − *Dr. Bing Zhang Department of Statistics, University of Kentucky, Lexington, Kentucky 40536, United States*

Siqi Guan − *Kentucky Tobacco Research and Development Center, University of Kentucky, Lexington, Kentucky 40546, United States;* Present Address: Nitto Avecia Pharma Services, 6 Vanderbilt, Irvine, California 92618, United States

Ying Wu − *Kentucky Tobacco Research and Development Center, University of Kentucky, Lexington, Kentucky 40546, United States*

Complete contact information is available at: https://pubs.acs.org/10.1021/acs.chemrestox.3c00004

Funding

This project was supported by the U.S. Food and Drug Administration through grant RFA-FD-14-001.

Notes

The views expressed in this paper do not necessarily reflect the official policies of the Department of Health and Human Services nor does any mention of trade names, commercial practices, or organization imply endorsement by the United States Government.

The authors declare no competing financial interest.

■ ABBREVIATIONS

HPHC, harmful and potentially harmful constituents; TSNA, tobacco-specific nitrosamines; NNK, 4-(methynitrosamino)-1(3-pyridyl)-1-butanone; NNN, *N*-nitrosonornicotine; B[α]P, benzo[α]pyrene; NDHA, *N*-nitroso-di-*n*-hexylamine; Na_2HPO_4, disodium hydrogen phosphate; NaOH, sodium hydroxide; MTBE, methyl tertiary-butyl ether; CO, carbon monoxide; TPM, total particulate matter; Vf, filter region ventilation; Vo, overall ventilation; FDA, US Food and Drug Administration; ISO, International Organization for Standardization; CTRP, the Center of Tobacco Reference Products

■ REFERENCES

(1) CDC. *Health Effects of Cigarette Smoking*. https://www.cdc.gov/tobacco/data_statistics/fact_sheets/health_effects/effects_cig_smoking/index.htm (accessed April 13, 2020).

(2) CDC. *Current Cigarette Smoking Among Adults in the United States*. https://www.cdc.gov/tobacco/data_statistics/fact_sheets/adult_data/cig_smoking/index.htm (accessed April 13, 2020).

(3) FDA. *Reporting Harmful and Potentially Harmful Constituents in Tobacco Products and Tobacco Smoke Under Section 904(a)(3) of the Federal Food, Drug, and Cosmetic Act* https://www.fda.gov/media/83375/download (accessed May 9, 2016).

(4) FDA. *Proposed Rule: Premarket Tobacco Product Applications and Recordkeeping Requirements* https://www.federalregister.gov/documents/2019/09/25/2019-20315/premarket-tobacco-product-applications-and-recordkeeping-requirements (accessed April 13, 2020).

(5) Caruso, M.; Distefano, A.; Emma, R.; Zuccarello, P.; Copat, C.; Ferrante, M.; et al. In vitro cytoxicity profile of e-cigarette liquid samples on primary human bronchial epithelial cells. *Drug Test Anal.* **2022**, 1−11.

(6) Ji, H.; Jin, Z. Analysis of six aromatic amines in the mainstream smoke of tobacco products. *Anal Bioanal Chem.* **2022**, *414*, 4227−4234.

(7) Dalrymple, A.; Bean, E. J.; Badrock, T. C.; Weidman, R. A.; Thissen, J.; Coburn, S.; et al. Enamel staining with e-cigarettes, tobacco heating products and modern oral nicotine products compared with cigarettes and snus: An in vitro study. *Am. J. Dent.* **2021**, *34* (1), 3−9.

(8) Sakai, Y.; Mori, S.; Yanagimachi, M.; Takahashi, T.; Shibuya, K.; Kumagai, A.; et al. Inter-Laboratory Reproducibility and Interchangeability of 3R4F and 1R6F Reference Cigarettes in Mainstream Smoke Chemical Analysis and in Vitro Toxicity Assays. *Beitrage zur Tab Int. Contrib to Tob Res.* **2020**, *29* (3), 119−35.

(9) Jaccard, G.; Djoko, D. T.; Korneliou, A.; Stabbert, R.; Belushkin, M.; Esposito, M. Mainstream smoke constituents and in vitro toxicity comparative analysis of 3R4F and 1R6F reference cigarettes. *Toxicol Reports* **2019**, *6*, 222−231.

(10) Chapman, G. M.; Bravo, R.; Stanelle, R. D.; Watson, C. H.; Valentin-Blasini, L. Sensitive and selective gas chromatography-tandem mass spectrometry method for the detection of nitrobenzene in tobacco smoke. *J. Chromatography A* **2018**, *1565*, 124−129.

(11) ISO. *ISO Guide 35:2017. Reference materials − General and statistical principles for certification*, 2017.

(12) ISO. *ISO 3402:1999 Tobacco and tobacco products − Atmosphere for conditioning and testing*, 1999.

(13) ISO. *ISO 3308:2012 Routine analytical cigarette-smoking machine — Definitions and standard conditions*, 2012.

(14) ISO. *ISO 4387:2019 Cigarettes — Determination of total and nicotine-free dry particulate matter using a routine analytical smoking machine*, 2019.

(15) CORESTA. *CORESTA Recommended Method 58. Determination of Benzo[a]pyrene in Cigarette Mainstream Smoke by Gas Chromatography-Mass Spectrometry*. https://www.coresta.org/sites/default/files/technical_documents/main/CRM_58-Nov2019.pdf (accessed April 13, 2020).

(16) *Reference Material Data Sheet RT1 1R6F Ground Filler*. https://ctrp.uky.edu/assets/pdf/webdocs/RT1_Data_Sheet_(1R6F_Ground_Filler).pdf (accessed March 1, 2017).

(17) Mascha, E.; Sessler, D. Equivalence and Noninferiority Testing in Regression Models and Repeated-Measures Designs. *Anesthesia & Analgesia* **2011**, *112* (3), 678−687.

(18) Van De Merbel, N.; Savoie, N.; Yadav, M.; et al. Stability: Recommendation for best practices and harmonization from the global bioanalysis consortium harmonization team. *AAPS J.* **2014**, *16* (3), 392−9.

(19) *Certificate of Analysis 1R6F Certified Reference Cigarette*. https://ctrp.uky.edu/assets/pdf/webdocs/CoA18_1R6F.pdf (accessed March 1, 2017).

(20) Huang, H. Y.; Hsieh, S. H. Analyses of tobacco alkaloids by cation-selective exhaustive injection sweeping microemulsion electrokinetic chromatography. *J. Chromatogr A* **2007**, *1164*, 313−9.

(21) Hoffmann, D.; Adams, J. D. Carcinogenic Tobacco-specific N-Nitrosamines in Snuff and in the Saliva of Snuff Dippers. *Cancer Res.* **1981**, *41*, 4305−8.

(22) Foiles, P. G.; Akerkar, S. A.; Carmella, S. G.; et al. Mass Spectrometric Analysis of Tobacco-Specific Nitrosamine-DNA Adducts in Smokers and Nonsmokers. *Chem. Res. Toxicol.* **1991**, *4*, 364−8.

(23) Gelhaus, S. L.; Harvey, R. G.; Penning, T. M.; Blair, I. A. Regulation of benzo[a]pyrene-mediated dna-and glutathione-adduct formation by 2,3,7,8-tetrachlorodibenzo-p -dioxin in human lung cells. *Chem. Res. Toxicol.* **2011**, *24* (1), 89−98.

(24) *Factors Affecting the Rate of Evaporation*. https://byjus.com/chemistry/factors-affecting-rate-of-evaporation/ (accessed February 16, 2023).

(25) Harris, F. S.; Robinson, J. S. Factors affecting the evaporation of moisture from the soil. *J. Agric Res.* **1916**, *VII* (10), 439−461.

(26) Jimenez, C.; Ventura, R.; Segura, J.; et al. Protocols for stability and homogeneity studies of drugs for its application to doping control. *Analytical Chimica Acta* **2004**, *515*, 323−331.

(27) U.S. Department of Health and Human Services, Food and Drug Administration, Center for Drug Evaluation and Research (CDER), Center for Veterinary Medicine (CMV). *Guidance for Industry, Bioanalytical Method Validation*, 2018.

(28) U.S. Department of Health and Human Services, Food and Drug Administration, Center for Tobacco Products. *Guidance for Industry, Validation and Verification of Analytical Testing Methods Used for Tobacco Products*, 2021.

(29) Bao, M.; Joza, P. J.; Masters, A.; Rickert, W. S.; et al. Analysis of Selected Carbonyl Compounds in Tobacco Samples by Using Pentafluorobenzylhydroxylamine Derivatization and Gas Chromatography-Mass Spectrometry. *Contributions to Tobacco Research* **2014**, *26*, 86−97.

International Journal of Biological Macromolecules 252 (2023) 126472

Contents lists available at ScienceDirect

International Journal of Biological Macromolecules

journal homepage: www.elsevier.com/locate/ijbiomac

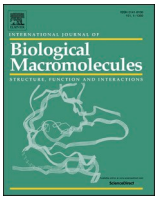

Partial desensitization of MYC2 transcription factor alters the interaction with jasmonate signaling components and affects specialized metabolism

Xin Hou [a], Sanjay Kumar Singh [b], Joshua R. Werkman [b], Yongliang Liu [b], Qinghua Yuan [c], Xia Wu [b], Barunava Patra [b], Xueyi Sui [d], Ruiqing Lyu [b], Bingwu Wang [d], Xiaoyu Liu [e], Yongqing Li [f], Wei Ma [g], Sitakanta Pattanaik [b,*], Ling Yuan [b,*]

[a] Department of Tobacco, College of Plant Protection, Shandong Agricultural University, Shandong Province Key Laboratory of Agricultural Microbiology, Tai'an 271018, China
[b] Department of Plant and Soil Sciences, Kentucky Tobacco Research and Development Center, University of Kentucky, Lexington, KY 40546, USA
[c] Crop Research Institute, Guangdong Academy of Agricultural Sciences, Key Laboratory of Crop Genetic Improvement of Guangdong Province, Guangdong Provincial Engineering & Technology Research Center for Tobacco Breeding and Comprehensive Utilization, Guangzhou 510640, China
[d] Tobacco Breeding and Biotechnology Center, Yunnan Academy of Tobacco Agricultural Sciences, Kunming 650021, Yunnan, China
[e] Pomology Institute, Shanxi Agricultural University, Taigu 030815, Shanxi, China
[f] Key Laboratory of South China Agricultural Plant Molecular Analysis and Genetic Improvement, Guangdong Provincial Key Laboratory of Applied Botany, South China Botanical Garden, Chinese Academy of Sciences, Guangzhou 510520, China
[g] School of Biological Sciences, Nanyang Technological University, Singapore 637551, Singapore

ARTICLE INFO

Keywords:
Transcriptional regulation
Protein-protein interaction
MYC2
MEDIATOR25
Homology structural modeling
Specialized metabolism

ABSTRACT

The activity of bHLH transcription factor MYC2, a key regulator in jasmonate signaling and plant specialized metabolism, is sensitive to repression by JASMONATE-ZIM-domain (JAZ) proteins and co-activation by the mediator subunit MED25. The substitution of a conserved aspartic acid (D) to asparagine (N) in the JAZ-interacting domain (JID) of Arabidopsis MYC2 affects interaction with JAZ, although the mechanism remained unclear. The effects of the conserved residue MYC2^{D128} on interaction with MED25 have not been investigated. Using tobacco as a model, we generated all possible substitutions of aspartic acid 128 (D128) in NtMYC2a. NtMYC2a^{D128N} partially desensitized the repression by JAZ proteins, while strongly interacting with MED25, resulting in increased expression of nicotine pathway genes and nicotine accumulation in tobacco hairy roots overexpressing NtMYC2a^{D128N} compared to those overexpressing NtMYC2a. The proline substitution, NtMYC2a^{D128P}, negatively affected transactivation and abolished the interaction with JAZ proteins and MED25. Structural modeling and simulation suggest that the overall stability of the JID binding pocket is a predominant cause for the observed effects of substitutions at D128. The D128N substitution has an overall stabilizing effect on the binding pocket, which is destabilized by D128P. Our study offers an innovative tool to increase the production of plant natural products.

1. Introduction

The plant basic helix-loop-helix transcription factors (bHLH TFs) are one of the largest TF families and regulate many biological processes, including growth and development, phytohormone signaling, defense response, and biosynthesis of specialized metabolites [1–3]. The Arabidopsis bHLH TF family is divided into 12 subgroups based on amino acid sequence alignment of the bHLH domain, and the subgroup IIIe has four members, MYC2, MYC3, MYC4 and MYC5 (bHLH028) [2]. Overall, the exact mechanisms by which MYCs regulate metabolic pathway genes are complex and not fully understood. MYC2, MYC3, MYC4, and MYC5, are known to interact with the jasmonate ZIM domain (JAZ) proteins that are repressors of jasmonate signaling [4–6]. In the absence of exogenous jasmonate (JA) or low endogenous JA, the JAZ proteins form complexes with MYC2 that repress its activity by recruiting the core-repressor TPL (TOPLESS) through the adaptor protein NINJA (NOVEL INTERACTOR OF JAZ) [7]. Upon the perception of JA, the JAZ proteins bind to the JA co-receptor COI1 (CORONATINE INSENSITIVE1) and are

* Corresponding authors at: Department of Plant and Soil Sciences, Kentucky Tobacco Research and Development Center, University of Kentucky, Lexington, KY 40546, USA.
E-mail addresses: spatt2@uky.edu (S. Pattanaik), lyuan3@uky.edu (L. Yuan).

https://doi.org/10.1016/j.ijbiomac.2023.126472
Received 14 April 2023; Received in revised form 20 August 2023; Accepted 21 August 2023
Available online 23 August 2023

subsequently degraded by the 26S/ubiquitin proteasome system (26S/UPS), thus releasing MYC2 from repression [4,8,9]. The de-repression of MYC2 leads to the activation of downstream genes, and this mechanism is well conserved across many plant species [3]. The JAZ proteins contain two highly conserved domains: ZIM and Jas domain. The ZIM domain mediates homo- and hetero-dimerization of JAZ proteins. The Jas domain is crucial for interaction with COI1, MYC2, and R2R3MYBs [8,10]. In addition to the C-terminal Jas domain, an N-terminal cryptic MYC-interaction domain (CMID) has been identified in a few Arabidopsis JAZ proteins, including JAZ1, 2, 5, 6 and 10 [11,12].

A conserved JAZ Interaction Domain (JID) at the N-termini of MYC TFs is important for MYC-JAZ interaction [5]. In Arabidopsis, both JID and the transactivation domain (TAD) of MYC3 are involved in the interaction with JAZ proteins [13]. The aspartic acid (D) to asparagine (N) mutation at amino acid 94 (D94N) in the MYC3 JID affects the interaction with JAZ proteins [14]. In addition, the analogous mutation (D105N) in Arabidopsis MYC2 also abolishes its interaction with several JAZ proteins [14]. The JID-TAD of AtMYC2 and AtMYC3 is also important for the interaction with MEDIATOR25 (MED25), a subunit of the Mediator transcriptional coactivator complex and a key component of the JA signaling pathway [15,16]. Arabidopsis MED25 contains a von Willebrand factor type A (vWFA) domain at the N-terminus followed by a non-conserved middle domain (MD), an activator-interacting domain (ACID), and a C-terminus glutamine-rich domain (GD) [16]. ACID of AtMED25 is essential for interaction with TFs including AtMYC2 [16]. The impact of the D-to-N mutation on the MYC2-MED25 interaction has not been studied.

JA signaling plays a universal role in the plant kingdom and regulates plant growth, development, defense against herbivores and necrotrophs, metabolism, and interaction with the environment [17,18]. MYC2 is a key component in the JA-signaling pathway and a key regulator of biosynthesis of plant specialized metabolites, such as artemisinin in *Artemisia annua* [19], paclitaxel in *Taxus cuspidata* [20], terpenoid indole alkaloids (TIAs) in *Catharanthus roseus* [21–23], and nicotine and other specialized metabolites in tobacco [24–29]. The conserved regulatory roles of MYC2 across plant species prompted us to further explore the potential effects of mutations in MYC2 JID in the regulation of specialized metabolism using tobacco as a model and to gain structural insights into MYC2 interaction with the JA signaling components. Nicotine biosynthesis is regulated by the JA-responsive *NICOTINE1* (*NIC1*) and *NIC2* loci APETALA2/ETHYLENE RESPONSE FACTORS (AP2/ERFs), as well as NtMYC2 [24,27,30,31]. Three full-length cDNA sequences, designated as NtMYC2a, NtMYC2b, and NtMYC2c, have been identified in tobacco [28]. NtMYC2a and NtMYC2b of the tetraploid tobacco are likely originated from the two progenitors, *Nicotiana tomentosiformis* and *N. sylvestris*, and NtMYC2b and NtMYC2c appear to be allelic as the amino acid sequences are identical [28]. NtMYC2s act upstream of the *NIC* loci AP2/ERFs, such as ERF189, ERF199, and ERF221, to regulate their expression. In addition, NtMYC2s co-regulate key genes in the nicotine biosynthetic pathway, such as *quinolinate phosphoribosyltransferase* (*QPT*) and *putrescine N-methyltransferase* (*PMT*), with the *NIC* loci AP2/ERFs [25,28]. The JAZ proteins are negative regulators of the nicotine biosynthetic pathway [32]. Here, using saturation mutagenesis, protein-protein interaction assay, transactivation assay, and protein structural modeling, we demonstrated that the mutation of the conserved aspartic acid (D128) in JID of NtMYC2a affects its interaction with tobacco NtJAZ proteins and alters the transactivation activity on key nicotine pathway gene promoters. The proline substitution, NtMYC2a^{D128P}, negatively affected transactivation and abolished the interaction with NtJAZ proteins. As the JID-TAD of MYC2 is important for the interaction with MED25, we sought to find out whether the mutations to MYC2^{D128} also affect the interaction with NtMED25. All substitutions except proline (NtMYC2a^{D128P}) interacted with MED25. The homology modeling and structural simulation provided insights into the structural basis of protein-protein interaction between NtMYC2a and NtJAZ or NtMED25. In addition, we showed that overexpression of *NtMYC2a*^{D128N} in tobacco hairy roots enhanced the expression of nicotine pathway genes and increased nicotine accumulation compared to *NtMYC2a* overexpression. Transcriptional regulation of many plant specialized metabolic pathways are well conserved across the species, and our work provides an innovative approach to engineering metabolic pathways to increase the production of medicinal compounds by targeting the ability of a TF to interact with co-regulators.

2. Materials and methods

2.1. Plant material and cell line

Nicotiana tabacum var. *Samsun*NN was used for gene cloning and generation of transgenic hairy roots. *N. tabacum* var. Xanthi cell line was used for protoplast-based promoter assays [33,34].

2.2. Analysis of tobacco transcriptomes

RNA-seq data of different tobacco tissues (leaf, stem, and root) were obtained from the sequence read archive database (SRA; Accession No. PRJNA208209) [35]. RNA-seq data of tobacco roots untreated (control) and treated with JA (100 μM) for 0.5 h, 1 h, 2 h and 4 h, were generated in-house [36]. The low-quality reads were processed using the prinseq-lite-0.20.4 [37], and qualities of the pre-processed reads were assessed using FastQC (version 0.11.3; Babraham Bioinformatics, Cambridge, UK). Bowtie2 was used for read mapping [38] using the reference tobacco genome sequence from the Sol Genomics Network database [39]. The log2 Fragments Per Kilobase of transcript per Million mapped reads (FPKM) was used for clustering calculation and visualization by *ComplexHeatmap* packages in R (https://www.R-project.org/; [40].

2.3. Saturation mutagenesis

The aspartic acid (D128) of NtMYC2a was mutated to all 19 amino acids by PCR-based site-saturated mutagenesis [41]. Mutations were confirmed by sequencing of individual clones.

2.4. Gene cloning, vector construction and luciferase assay

Isolation of protoplasts from tobacco cell cultures and protoplast electroporation were performed as previously described [41]. The reporter plasmids for protoplast assays were made by cloning the *PMT* (1500 bp) [34,42], *QPT* (1579 bp) [34,43], *BBL* (*berberine bridge enzyme-like; 1200 bp*) and *MATE1* (*multidrug and toxic compound extrusion 1;* 1030 bp) [44] promoters into a vector containing the firefly *luciferase* (*LUC*) and *rbcS* terminator. The effector plasmids were constructed by cloning *NtMYC2a* and *NtMYC2a* mutants into a modified pBS vector under the control of the *CaMV*35S promoter and *rbcS* terminator. The *CaMV*35S promoter and *rbcS* terminator driven β-glucuronidase (*GUS*) reporter was used as an internal control in the protoplast assay. Tobacco protoplasts were electroporated with the reporter, effector, and internal control plasmids in different combinations; LUC and GUS activities in electroporated protoplasts were measured as described previously [41].

2.5. Yeast two-hybrid assay

The full-length cDNA of *NtMYC2a*, *NtMYC2a* mutants, *NtJAZ1*, *NtJAZ2*, *NtJAZ3*, *NtJAZ8* and *NtTPL* were cloned in pAD-GAL4–2.1 and *NtMED25*, *NtJAZ1, NtJAZ2, NtJAZ3*, *NtJAZ8* and *NtNINJA* in pBD-GAL4 Cam (Stratagene, USA). *C. roseus* MYC2 D126N mutant (*CrMYC2a*^{D126N}) mutant generated in our previous study [34] was cloned in pAD-GAL4–2.1. The *C. roseus* JAZ proteins were cloned in pBD-GAL4 as described previously [21]. The bait and prey plasmids were co-transformed into yeast strain *AH109* and selected on synthetic dropout (SD) medium lacking leucine and tryptophan (−leu-trp, −LT). Protein-

protein interactions were detected by streaking the transformed colonies on SD medium lacking adenine, histidine, leucine, tryptophan (−ade-his-leu-trp) or -his-leu-trp.

2.6. Construction of plant expression vectors and transformation

For generation of hairy roots, *NtMYC2a* and *NtMYC2a*^{D128N} were cloned into the binary vector pCAMBIA2301 containing the *CaMV*35S promoter and *rbcS* terminator. An empty pCAMBIA2301 vector (EV) served as the control. The plasmids were mobilized into *Agrobacterium rhizogenes* R1000 stain by freeze-thaw [45]. Tobacco leaf discs were used for generation of hairy roots as described previously [33,34]. The transgenic status of the hairy root lines was verified by RT-PCR amplification of *rolB*, *rolC, Vir, GUS* and *nptII* (*neomycin phosphotransferase*). Independent hairy root lines with comparable expression of *NtMYC2a* and *NtMYC2a*^{D128N} were selected for further analysis. Primers used in this study are listed in Table S1.

2.7. RNA isolation, gene expression analysis and alkaloid quantification

RNA was isolated from empty vector (EV) control, *NtMYC2a* and *NtMYC2a*^{D128N} overexpressing hairy roots and roots of transgenic plant using RNeasy Plant Mini Kit (QIAGEN, USA) and used for first-strand cDNA synthesis. To verify JA-induced expression of *NtMYC2a* and *NtJAZs*, and *NtMED25* tobacco roots treated with 100 μM methyl jasmonate (MeJA; Sigma-Aldrich, USA) for 2 h were used RNA isolation and cDNA synthesis. Reverse transcription quantitative PCR (RT-qPCR) (RT-qPCR) was performed as previously described [21]. The $2^{-\Delta\Delta CT}$ (cycle threshold) method was used to measure transcript levels [46]. Tobacco *EF1α* (GenBank accession number D63396) was used as an internal control [33,47]. The primers used in RT-qPCR are listed in Table S1. Nicotine contents in transgenic hairy roots were measured as previously described [33,34].

2.8. Homology modeling and molecular dynamics

Homology modeling of NtMYC2a was performed via the SWISS-MODEL server against a user aligned template with 4rru.1.A (5–242) [13], and the subsequent model was built with ProMod3 3.2.0 [48]. Residue 128 was mutated to the desired amino acids via line editing. The models were obtained and visually verified using PyMol. Molecular dynamic setup and simulations were performed with AmberTools21 and Amber20 [49], respectively. The ff19SB force field was utilized, and OPC waters were added to a distance 10 Å beyond the protein. Protein charge was neutralized with either sodium or chloride ions, and the sodium chloride concentration was set to 150 mM. Stepped minimization, heating (300K), and equilibration of the system were performed before production runs of 100 ns (nanosecond). To identify and sort secondary structure confirmations via intra-backbone hydrogen bonds, Dictionary of Secondary Structures in Proteins (DSSP) analysis was performed in cpptraj [49,50]. Confirmation frequency was determined by sorting and counting the identified confirmations of each residue for each frame in the simulation from DSSP output. If a residue could not match hydrogen bonding criteria for a known secondary structure confirmation, the residue was classified as “none” for no identifiable structure. Output was graphed as position (residue) over time with the secondary structure colored by type. The NtMED25 acidic domain (540–682) was modeled using ab initio protein structure assembly via C-QUARK to obtain a suitable structure to explore how NtMED25 interacts with NtMYC2a in the JID binding pocket [51].

2.9. Statistical analysis

Data on luciferase assay, RT-qPCR and nicotine contents are from three independent experiments or three biological replicates. The Student’s *t*-test or one-way ANOVA and Tukey’s HSD test for multiple comparisons was used for data analysis. The significance levels (*P* values) are included in the figure legends.

3. Results

3.1. JA-inducible NtMYC2s contain highly conserved JID-TAD

NtMYC2a shares 98 % amino sequence identity with NtMYC2b and 53–67 % amino acid sequence identity with those of Arabidopsis and *C. roseus* MYC2s, respectively (Fig. S1). The JAZ-interaction domain-transactivation domain (JID-TAD) and the bHLH domain are highly conserved among all MYC2 proteins. JID-TAD is essential for interaction with the JAZ proteins, whereas the bHLH domain is required for DNA binding and dimerization [3,5,13]. The JID-TAD of NtMYC2a shares 67 % and 82 % sequence identity with Arabidopsis and *C. roseus* MYC2, respectively (Fig. S1). To determine the expression profile of *NtMYC2s*, we analyzed the transcriptomes of different tobacco tissues. As shown in Fig. 1A, expression of *NtMYC2a* and *NtMYC2b* was significantly higher in stems compared to leaves and roots. MYC2 is a central regulator of JA signaling and its expression is induced by JA [3]. Analysis of time-course root transcriptomes revealed that the expression of *NtMYC2a* and *NtMYC2b* was induced significantly within 0.5 h after JA induction and then decreased gradually (Fig. 1B). As expected, the expression of nicotine pathway genes was also induced by JA (Fig. 1B). JA-induced expression of *NtMYC2a* was further verified in tobacco roots treated with JA using RT-qPCR. *NtMYC2a* expression was induced 3.5-fold compared to the control (Fig. 1C).

3.2. JA-responsive tobacco JAZs are highly expressed in roots

The Arabidopsis and *C. roseus* JAZ1, JAZ2, JAZ3, JAZ8 and JAZ10 are well characterized for their roles in JA signaling and specialized metabolism [4,9,12,21,52]. Tobacco JAZ1 and JAZ2 were reported previously [32]. We identified the tobacco JAZ3 and JAZ8. A true homologue of Arabidopsis or *C. roseus* JAZ10 was not found in the tobacco genome. Tobacco JAZ1, JAZ2, JAZ3 and JAZ8 share 29, 41, 32, and 55 % amino acid sequence identity with their Arabidopsis and *C. roseus* homologs, respectively (Fig. S2). The sequence identity is mostly limited to the conserved ZIM and Jas domains. We next analyzed the tobacco transcriptome to determine expression profiles of NtJAZs in leaf, stem and root tissues. Similar to the nicotine pathway genes, expression of all four NtJAZs is significantly higher in the root compared to the leaf and stem (Fig. 1A). We analyzed the expression of NtJAZs in transcriptomes of JA-treated tobacco roots. As shown in Fig. 1B, expression of all four NtJAZs was significantly induced by JA compared to the untreated control. Similar to *NtMYC2*, *NtJAZ1* expression was significantly induced within 0.5 h of JA treatment, whereas that of *NtJAZ2, NtJAZ3* and *NtJAZ8* was induced gradually and peaked at 4 h (Fig. 1B). JA-responsive expression of NtJAZs in tobacco roots was verified using RT-qPCR (Fig. 1C).

3.3. D128N and other substitutions of NtMYC2a differentially interact with JAZ proteins

The alignment of the amino acid sequences of the MYC2 JID domains from 50 monocot and dicot plant species showed that the analogous aspartic acid to D128 is almost completely conserved (Fig. S3). Based on the information generated from Arabidopsis MYC2^{D105N}, we reasoned that the corresponding mutation in NtMYC2a will likely affect the interaction with tobacco JAZs. We, therefore, generated NtMYC2a^{D128N} by site-directed mutagenesis and compared the interaction of NtMYC2a or NtMYC2a^{D128N} with the four tobacco JAZ proteins in yeast cells (Fig. 2A). Sequence alignment of the Jas domains of Arabidopsis, *C. roseus* and tobacco JAZs showed that amino acid residues previously reported to be critical for interaction with MYC2/MYC3 [13] are well conserved (Fig. 2B). As shown in Fig. 2C, NtMYC2a interacted with all

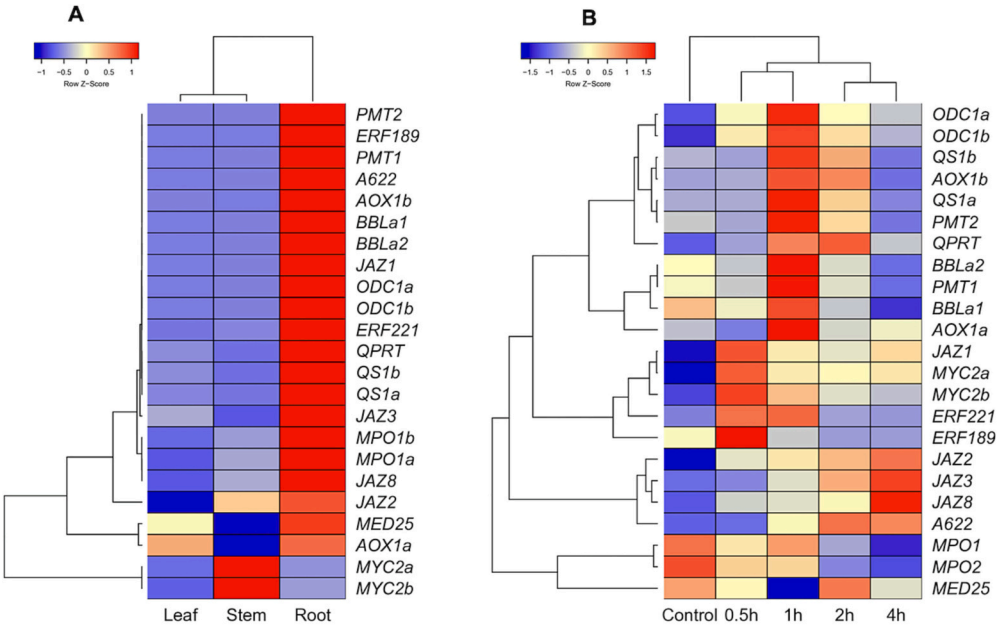

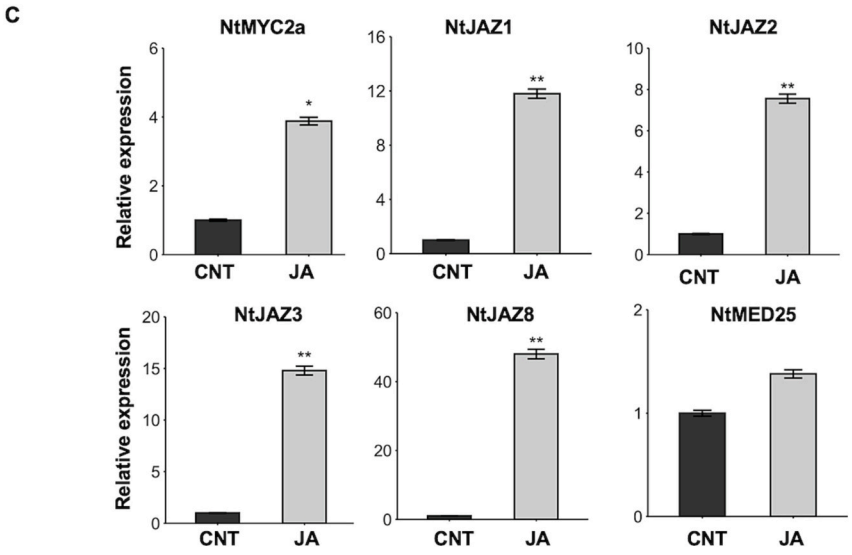

Fig. 1. Co-expression analysis of nicotine pathway genes and regulators in different tissues and the responses of tobacco MYC2, JAZs, and MED25 to JA induction. A. A heatmap shows expression profiles of *NtJAZs*, *NtMYC2a* and nicotine pathway genes in the leaf, stem and root. Transcriptomes of different tissues were used for co-expression analysis. B. A heatmap shows expression profiles of *NtJAZs*, *NtMYC2a* and nicotine pathway genes in JA-treated tobacco roots. Transcriptomes of tobacco roots treated with JA for 0.5 h, 1 h, 2 h and 4 h were used for co-expression analysis. Mock-treated sample served as control. C. Relative expression of *NtMYC2a, NtJAZ1*, *NtJAZ2, NtJAZ3*, *NtJAZ8*, *and NtMED25* in control (CNT) and MeJA-treated (2 h) tobacco roots, measured using RT–qPCR. Tobacco *EF1α* was used as an internal control. Data of three biological samples with mean ± SD of three biological samples are presented. Student's *t*-test was used for calculating the statistical significance: *, $P < 0.05$; **, $P < 0.01$.

four JAZ proteins, evident by the growth of yeast cells on the quadruple selection medium (SD-AHLT). However, the D128N mutation (NtMYC2a^{D128N}) abolished its ability to interact with NtJAZ2 and NtJAZ3, but not with NtJAZ1 and NtJAZ8 (Fig. 2C). The interaction of NtMYC2a or NtMYC2a^{D128N} with JAZ3 was further validated in a plant cell-based assay. The luciferase (LUC) reporter fused to five tandem repeats of the GAL response element (5× GALRE) was electroporated into tobacco cells, alone or in combination, with vectors expressing BD-NtMYC2a, BD-NtMYC2a^{D128N}, and JAZ3. JAZ3 was chosen as it interacts with NtMYC2a, but not NtMYC2a^{D128N} (Fig. 2C). Expression of BD-NtMYC2a or BD-NtMYC2a^{D128N}, significantly activated the luciferase activity, while co-expression of BD-NtMYC2a and JAZ3 reduced the LUC activity by ~35 %, and the LUC activity was reduced marginally (~15 %) when JAZ3 was co-expressed with *NtMYC2a*^{D128N} (Fig. 2D).

Our results support the notion that D128N affects the interaction of NtMYC2a with JAZ proteins; however, the structural basis for the critical role of D128 remained unexplained. To determine whether the substitutions of D128 to other amino acids also affect the interaction with NtJAZs, we substituted D128 with all 19 possible amino acids by saturation mutagenesis and evaluated the interaction of the mutants with the four NtJAZ proteins. As shown in Table 1, except for alanine (A), glutamic acid (E), glycine (G), tryptophan (W) and leucine (L), mutations of D128 to other amino acids significantly affected the interaction with NtJAZ proteins.

3.4. The NtMED25 interaction with NtMYC2a^{D128} mutants

MED25 functions as a co-regulator of TFs through protein-protein interaction. To determine whether NtMED25 interacts with NtMYC2a and mutations in the JID affect the interaction, we identified and cloned the tobacco MED25 (NtMED25). NtMED25 shares 62 % sequence identity with AtMED25 (Fig. S4) and contains all the conserved domains identified in AtMED25 (Fig. 3A). We measured *NtMED25* expression in JA-treated tobacco roots. Unlike *NtMYC2a*, *NtMED25* expression was not significantly altered by JA treatment (Fig. 1C). Yeast two-hybrid assay showed that NtMED25 interacts with NtMYC2a (Fig. 3B). All

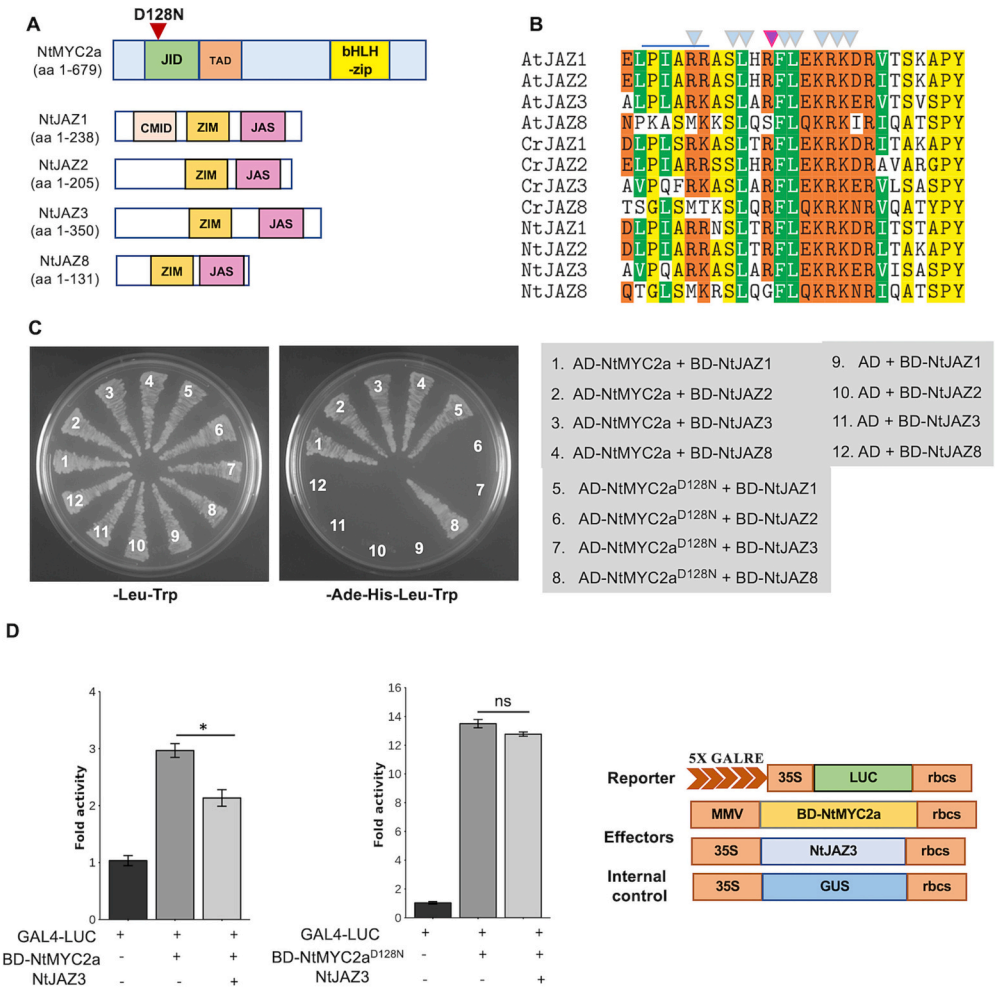

Fig. 2. Interaction of NtMYC2a and NtMYC2a^{D128N} with tobacco JAZ proteins in yeast and plant cells. A. Schematic diagrams showing the different domains of NtMYC2a (JID, TAD, bHLH) and NtJAZ1, NtJAZ2, NtJAZ3 and NtJAZ8 (ZIM and Jas) proteins. The aspartic acid to asparagine mutation (D128N) in the JID is indicated by a reverse triangle. B. Amino acid sequence alignment of the Jas domains of *A. thaliana* (*At*), *C. roseus* (*Cr*) and *N. tabacum* (*Nt*) JAZ proteins. Amino acids critical for interaction with MYC2 are indicated by reverse triangles (blue). The arginine (R) in the jas domain of AtJAZ9 that forms charge interaction with aspartic acid (D94) in the AtMYC3 JID is indicated by a purple triangle. C. NtMYC2a and NtMYC2a^{D128N} fused to the GAL4 activation domain (AD) and the NtJAZ1, NtJAZ2, NTJAZ3, and NtJAZ8 fused to GAL4-binding domain (BD) were co-transformed into the yeast cell AH109 and selected on double (−Leu-Trp) selection medium. Protein-protein interactions were detected by the growth of yeast cells on a quadruple (−Ade-His-Leu-Trp) selection medium. D. NtMYC2a interacts with NtJAZ3 in tobacco cells. The firefly *luciferase* (*LUC*) reporter is driven by the minimal *CaMV35S* promoter fused to five tandem repeats of GAL response elements (5× GALRE). Tobacco protoplasts were electroporated with the reporter, alone or in combination, with effector BD-NtMYC2a, NtMYC2a^{D128N} and NtJAZ3. A *CaMV35S-GUS* served as internal control. LUC activity was normalized against GUS activity. Means ±SD of three independent experiments are presented. Student's *t*-test was used to calculate statistical significance: *, $P < 0.05$; Schematic diagram of the plasmids used in the protoplast assay are shown in right panel. bHLH, basic helix-loop-helix; CMID, cryptic MYC-interaction domain; JID, JAZ interaction domain; TAD, transactivation domain; ZIM, Zinc-finger protein expressed in Inflorescence Meristem.

amino acid substitutions of D128 in NtMYC2a did not affect the interaction with NtMED25, except for D128P which abolished the interaction (Fig. 3B and Table 2). The interaction between NtMED25 and NtMYC2a or MYC2a^{D128P} was further validated in plant cells. The LUC reporter (5XGALRE-35S-LUC) was electroporated into tobacco cells, alone or in combination, with vectors expressing BD-*NtMED25*, *NtMYC2a*, or *NtMYC2a^{D128P}*. Expression of BD-NtMED25 significantly activated LUC activity, and co-expression of *NtMYC2a* with BD-NtMED25 further increased the LUC activity, suggesting an interaction between NtMYC2a and NtMED25 in plant cells. However, LUC activity did not increase when *NtMYC2a^{D128P}* was co-expressed with *NtMED25* (Fig. 3C).

3.5. Long-distance effects in JID stability are seen using molecular dynamics

Three substituted models (D128N, D128I, and D128P) and a wild-type model (D128) of NtMYC2a in the apo form, without JAZ interaction partners, were run through molecular dynamics simulations for a length of 100 ns (Fig. 4A, Fig. S5A—C). The four panels in Fig. 4A show the evolution of the secondary structures of residue 120 to 134 (JID β2 strand) assigned by the DSSP algorithm as a function of simulation time (100 ns). Starting with position 128, the asparagine substitution, NtMYC2a^{D128N} was included because of its differential interaction with JAZ proteins via yeast two-hybrid assays and enhanced transactivation of select promoters. The isoleucine substitution, NtMYC2a^{D128I}, was included to represent a group of hydrophobic substitutions that do not interact with NtJAZ proteins, yet still interacted with NtMED25, unlike NtMYC2a^{D128P}. The NtMYC2a model (D128) showed that the β2 strand mostly remains in an extended beta-strand (blue) confirmation (93.7 % of the time; Fig. 4A) with minimal bending (red) throughout the length of the simulation. Even less structural variation was shown for NtMYC2a^{D128N} (D128N) as indicated by consistent blue (extended β-strand; 97.9 %) throughout the simulation, suggesting that the N substitution stabilized the β2 strand. However, major structural changes in the β2 strand of NtMYC2a^{D128I} (D128I) and NtMYC2a^{D128P} (D128P) were observed (Fig. 4A). Compared to the D128 model, the extended β-strand was disrupted by unassigned structures 58.9 % of the time (none, dark blue) in the D128I model. In the D128P model, the extended β-strand was disrupted by unassignable structures 57.2 % of the time (none, dark blue) and additionally disrupted by bending (red) 42.7 % of the time.

We further quantified the confirmation frequency of several key residues, within the β2 strand (Fig. 4B and C) and in α4 (Fig. 4D) and α3 (Fig. 4E) helixes that co-form the binding pocket with the β2 strand (Fig. 4F). Bending of the β2 strand was observed for the D128P model

Table 1
Interaction of NtMYC2a^{D128} site-saturated mutants with NtJAZ proteins in yeast cells.

Media	SD-Leu-Trp				SD-Ade-His-Leu-Trp			
NtMYC2 mutants	JAZ1	JAZ2	JAZ3	JAZ8	JAZ1	JAZ2	JAZ3	JAZ8
D128 (WT)	+++	+++	+++	+++	+++	+++	+++	+++
D128A	+++	+++	+++	+++	+++	+++	+++	+++
D128R	+++	+++	+++	+++	−	−	−	−
D128N	+++	+++	+++	+++	+++	−	−	+++
D128C	+++	+++	+++	+++	++	++	++	+++
D128Q	+++	+++	+++	+++	+++	−	−	+
D128E	+++	+++	+++	+++	+++	+++	+++	+++
D128G	+++	+++	+++	+++	+++	+++	++	+++
D128H	+++	+++	+++	+++	+++	++	−	+++
D128I	+++	+++	+++	+++	−	−	−	−
D128L	+++	+++	+++	+++	+++	+++	+++	+++
D128K	+++	+++	+++	+++	−	−	−	−
D128M	+++	+++	+++	+++	−	−	−	+++
D128F	+++	+++	+++	+++	+++	+++	−	+++
D128P	+++	+++	+++	+++	−	−	−	−
D128S	+++	+++	+++	+++	+	−	−	++
D128T	+++	+++	+++	+++	+++	−	+++	+++
D128W	+++	+++	+++	+++	+++	+++	+++	+++
D128Y	+++	+++	+++	+++	+	−	−	+++
D128V	+++	+++	+++	+++	−	−	−	+

Interaction strength of NtMYC2a mutants with JAZs as determined by the growth of cells on quadruple selection medium (−Ade-His-Leu-Trp) is indicated by + sign. +++ strong; ++ medium; + weak, − interaction not detected.

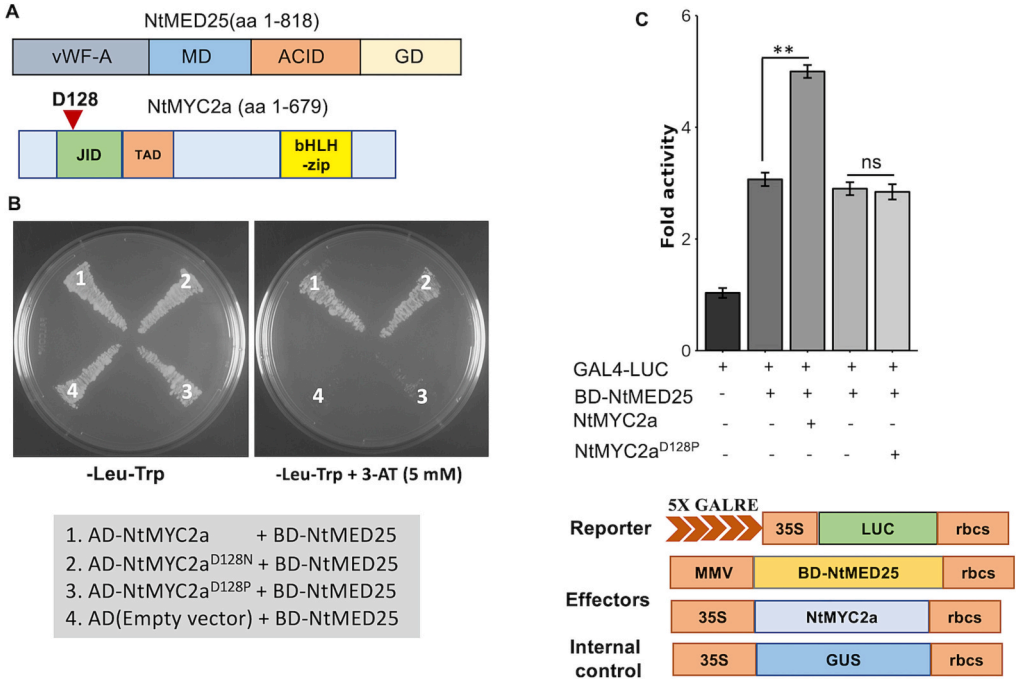

Fig. 3. Interaction of NtMYC2a and NtMYC2a mutants with tobacco MED25 in yeast and plant cells. A. Schematic diagrams showing the different domains of NtMYC2a (JID, TAD, bHLH) and NtMED25 (vWF-A, MD, ACID and GD). The aspartic acid (D128) in the JID is indicated by a reverse triangle. B. NtMYC2a fused to the GAL4 AD and NtMED25 fused to GAL4-BD were co-transformed into the yeast cell AH109 and selected on double (−Leu-Trp) selection plates. Protein-protein interactions were detected by the growth of yeast cells on quadruple SD-(-His-Leu-Trp + 5 mM 3AT) medium. C. NtMYC2a interacts with NtMED25 in tobacco cells. *LUC* reporter was fused to 5×-GALRE and the minimal *CaMV*35S promoter. The *LUC* reporter was electroporated into tobacco protoplasts, alone or in combination, with an effector BD-NtMED25 or NtMYC2a. A *CaMV*35S-*GUS* served as an internal control. Luciferase activity was normalized against GUS activity. Data from three independent experiments with means±SD are presented. Student's *t*-test was used for calculating statistical significance: **, $P < 0.01$; ACID, activator-interacting domain; GD, glutamine-rich domain (GD); MD, Non-conserved middle domain (MD); vWF-A, von Willebrand factor type A domain; 3-AT, 3-amino-1,2,4-triazole.

(yellow; Fig. 4B) that is consistent with the DSSP analysis (Fig. 4A). In comparison, for both D128wt and D128N models, the β2 strand is consistently extended β-strand (orange and blue bars; Fig. 4B). The secondary structure confirmation of NtMYC2a^{D128P} changed frequently, alternating between no identifiable secondary structure (dark blue) and a bend (red) (Fig. 4A). D128P also did not exist in a β-strand confirmation unlike the wildtype form (0.06 % vs 93.7 % of the time). This instability was propagated through the β2 strand. For example, W126 in the D128P model frequently alternated between an extended β-strand confirmation (13.2 %) and an unassignable confirmation (86.5 %; Fig. 4A and C), while the other three models remained between 95.5 % to 97.3 % extended β-strand.

Continuing around the JID binding pocket (Fig. 4F), DSSP analysis also found long-distance effects throughout the JID from the D128P and D128I substitutions in positions M193 and L163 (Fig. 4D, E). The residue, M193 (TAD; α4) (Fig. 4D), had an approximately three-fold increase in the 3_{10}-helix confirmation compared to the other three models (Fig. 4D). Further away, the α3 helix had multiple residue distortions

Table 2
Interaction of NtMYC2a^{D128} mutants with NtMED25 in yeast cells.

media	SD-Leu-Trp	SD-Leu-Trp-His +3-AT
NtMYC2 mutants	NtMED25	NtMED25
D128 (WT)	+++	+++
D128A	+++	+++
D128R	+++	+++
D128N	+++	+++
D128C	+++	+++
D128Q	+++	+++
D128E	+++	+++
D128G	+++	+++
D128H	+++	+++
D128I	+++	+++
D128L	+++	+++
D128K	+++	+++
D128M	+++	+++
D128F	+++	+++
D128P	+++	–
D128S	+++	+++
D128T	+++	+++
D128W	+++	+++
D128Y	+++	+++
D128V	+++	+++

Interaction strength of NtMYC2a mutants with NtMED25 as determined by the growth of cells on triple selection medium (-His-Leu-Trp + 3-AT) is indicated by + sign. – interaction not detected.

with the residue L163, possessing significant changes (Fig. 4E). Although predominantly existing in an α-helix confirmation, L163 showed the greatest variation away from an α-helix confirmation in the D128P model (32.5 % of the time in a turn confirmation; yellow), followed by the D128I model (12.5 % of the time in a turn confirmation; gray), compared to the D128 and D128N models (0.3 % and 0.1 %, respectively) which largely remained in an α-helix confirmation (Fig. 4E). These findings suggest that the D128N substitution has an overall stabilizing effect on the binding pocket, whereas D128I and D128P destabilize the binding pocket.

3.6. *NtMYC2a^{D128N} shows higher transactivation activity on the promoters of nicotine pathway genes in tobacco cells*

NtMYC2 is known to directly regulate key nicotine pathway genes (Fig. 5A). We, therefore, performed tobacco protoplast assay to determine whether the consequent inability of NtMYC2a mutants (NtMYC2a^{D128N}, NtMYC2a^{D128I}, NtMYC2a^{D128K}, NtMYC2a^{D128R}, and NtMYC2a^{D128P}) to interact with certain JAZ proteins affects the transactivation of the target promoters. The *LUC* reporter driven by the *QPT* promoter was electroporated into tobacco protoplasts, alone or in combination, with vectors expressing *NtMYC2a* or *NtMYC2a* mutants. As shown in Fig. 5B, transactivation of the *QPT* promoter by four of the five NtMYC2a mutants (with exception of D128P) was significantly higher (7–18 fold) than NtMYC2a. As activation of the *QPT* promoter by NtMYC2a^{D128N} was the highest (18-fold compared to control), NtMYC2a^{D128N} was selected to test for the activation of additional gene promoters, including those of *PMT*, and *BBL,* as well as the nicotine transporter *MATE1* (Fig. 5A). The *LUC* reporter driven by the promoters were electroporated into tobacco protoplasts, alone or in combination, with vectors expressing *NtMYC2a* or *NtMYC2a^{D128N}*. NtMYC2a activated the *BBL* and *MATE1* by 2- to 3.5-fold, but did not activate the *PMT* promoter, in tobacco protoplasts (Fig. 5C). The promoter activities were significantly higher (5 to 6-fold) when *NtMYC2a^{D128N}* was co-transformed with the *BBL,* or *MATE1* promoter compared to *NtMYC2a*. NtMYC2a^{D128N} activated the *PMT* promoter by 1.8-fold in tobacco cells compared to the control (Fig. 5C).

As transactivation of the *QPT* promoter by NtMYC2a and NtMYC2a^{D128N} was significantly higher compared to other promoters, we used it to further examine the combined effects of NtMYC2a, NtMYC2a^{D128N} and JAZ3. Tobacco cells were electroporated with *QPT-LUC*, alone or in combination, with vectors expressing *NtMYC2a*, *NtMYC2a^{D128N}* and *JAZ3*. JAZ3 interacts with NtMYC2a, but not NtMYC2a^{D128N} (Fig. 2C). Co-expression of *NtMYC2a* and *JAZ3*, significantly reduced (~41 %) the *QPT* promoter activity, while the activity was reduced marginally (~15 %) when *JAZ3* was co-expressed with *NtMYC2a^{D128N}* (Fig. 5D).

As NtMYC2a^{D128P} was unable to interact with NtJAZs or NtMED25 in yeast and plant cells, we sought to find out whether the NtMYC2a^{D128P} is produced and stable in the cell. We thus fused *NtMYC2a* or *NtMYC2a^{D128P}* to *LUC* to produce fusion proteins, NtMYC2a-LUC and NtMYC2a^{D128P}-LUC, and the LUC activity in tobacco cells was measured after electroporation. LUC activity of the fusion proteins indicated that similar to NtMYC2a, NtMYC2a^{D128P} is produced and stable in plant cells (Fig. S6A). We evaluated the transactivation activity of NtMYC2a^{D128P} on the nicotine pathway promoters in tobacco cells and found that NtMYC2a^{D128P} was unable to activate the promoters (Fig. S6B).

3.7. *NtMYC2a^{D128N} enhances expression of nicotine pathway genes and nicotine accumulation in hairy roots*

To substantiate the role of NtMYC2a^{D128N} in regulation of the nicotine pathway, we generated transgenic tobacco hairy roots overexpressing *NtMYC2a* or *NtMYC2a^{D128N}*. Hairy roots transformed with an empty vector (EV) served as a control. The transgenic status of the hairy roots was verified by RT-PCR (Fig. S7). After measuring the expression of *NtMYC2a* in transgenic hairy roots, two pairs of independent transgenic lines were selected, and in each pair, both *NtMYC2a* and *NtMYC2a^{D128N}* were expressed at comparable levels (in one pair both genes were expressed 4.4-5fold compared to control, and the other 13-15fold; Fig. 6). Expression of the nicotine pathway genes was increased by 3.5-25fold in *NtMYC2a* hairy root lines compared to EV; by comparison, overexpression of *NtMYC2a^{D128N}* resulted in a significant increase of the pathway gene expression (7–75 fold) compared to EV (Fig. 6). To determine the effects of increased expression on metabolic outcomes, we measured the nicotine contents in control, *NtMYC2a*, and *NtMYC2a^{D128N}* hairy roots. The nicotine accumulation was higher in *NtMYC2a^{D128N}* hairy roots compared to *NtMYC2a* roots (Fig. 6).

4. Discussion

TFs contain multiple distinct domains that are involved in DNA binding, protein-protein interaction and transcriptional activation or repression. A TF or TF complex commonly regulates most or all enzyme-encoding genes in a metabolic pathway, and the regulatory mechanism is well conserved across plant species. One classic example is the flavonoid biosynthetic pathway which is regulated by conserved MYB, bHLH, and WD40 TFs in many plant species [53] The *NIC1* and *NIC2* loci AP2/ERFs 189/199 and NtMYC2a jointly regulate nicotine biosynthesis in tobacco [25,27,28,30,54]. In *C. roseus*, CrMYC2 and orthologs of *NIC* locus AP2/ERFs, the ORCA TFs, regulate portions of the TIA pathway [23,34,55,56]. MYC2 and the GAME9/JRE4, orthologues of ORCAs, regulate steroidal glycoalkaloid biosynthesis in tomato and potato [57–59]. The modular nature and broad regulatory roles of TFs intrigue many to explore them for protein engineering and manipulation of metabolic pathways in plants for increasing the production of phytochemicals. Supporting this notion, we have previously shown that the transcriptional activities of two bHLH regulators of anthocyanin biosynthesis can be increased by laboratory-directed evolution [60]. A lysine (K) to methionine (M) substitution in the MYB-interacting region (MIR) of the perilla MYC-RP [61] and snapdragon DELILA [62] significantly increases the transactivation of both TFs in yeast and plant cells. Overexpression of the mutant, MYC-RP^{K157M} in tobacco increases anthocyanin accumulation in tobacco flowers compared to the wildtype TF [63]. The asparagine substitution of the conserved aspartic acid in the JID of MYC2 is of particular interest because the same mutation in

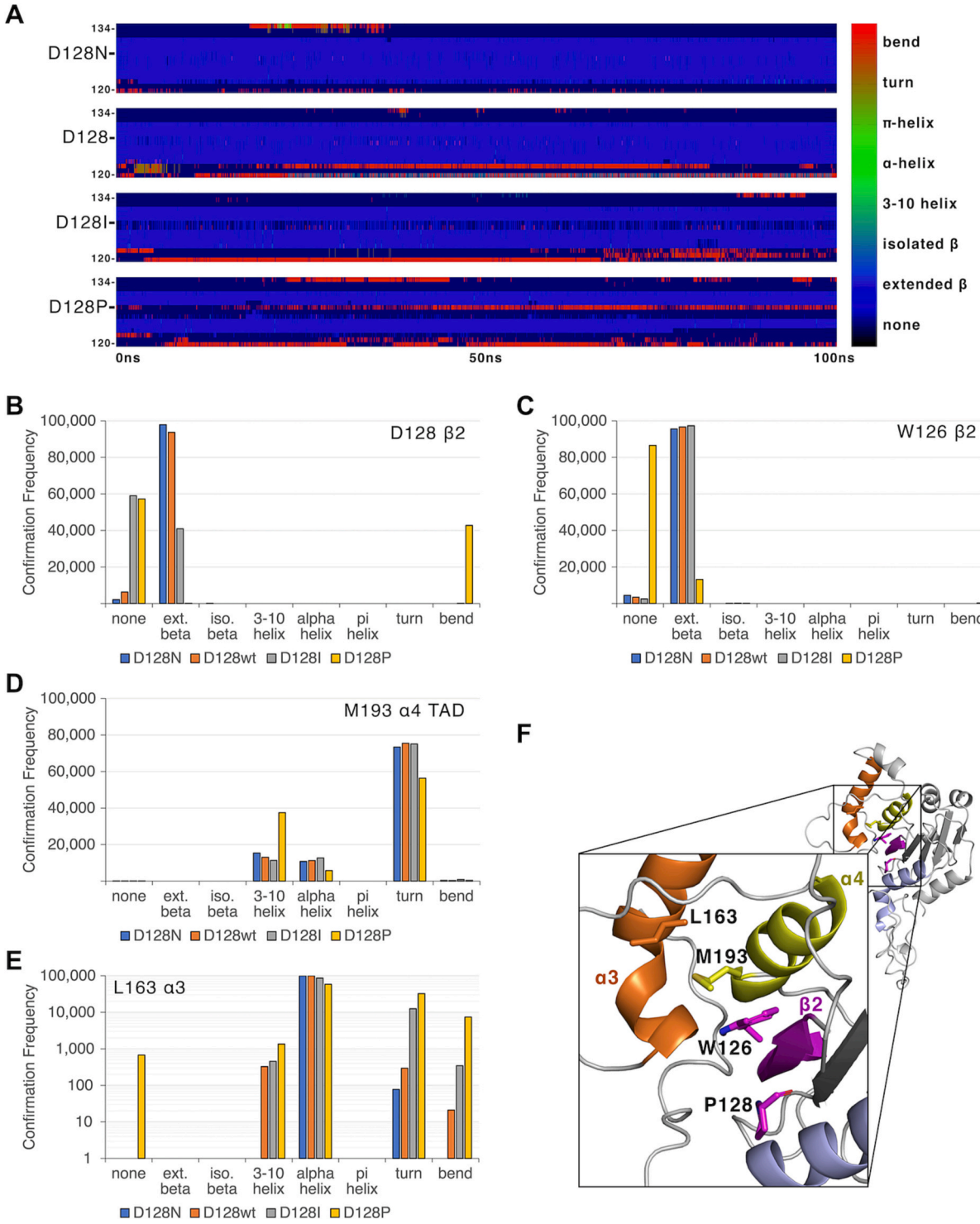

Fig. 4. Molecular dynamics simulations of apo NtMYC2a reveal changes in stability by selected substitutions of D128 of the β2-strand and long-distance effects of α4 and α3 to the JID binding pocket. A. Dictionary of Secondary Structures in Proteins (DSSP) analysis of the β2-strand (residues 120–134) of the apo NtMYC2a (D128), NtMYC2a^{D128N} (D128N), NtMYC2a^{D128I} (D128I) and NtMYC2a^{D128P} (D128P) shows the evolution of the secondary structures during the simulation of 100 ns. Each lined point in the graph represents a timepoint for a residue in the β2-strand. The colors represent the identified secondary structure for each residue, which allows visual observation of small or fast changes in the β2-strand over the course of time. Compared to NtMYC2a, stability increased in NtMYC2a^{D128N} (D128N) and decreased in NtMYC2a^{D128P} (D128P). Another hydrophobic amino acid (isoleucine) substitution (D128I) showed decreased stability but to a lesser extent compared to D128P. B. The confirmation frequency of D128 of the β2-strands for D128N, D128 (D128wt), D128I, and D128P. D128P shows the most significant changes from extended β-strand to bending. C. Position W126 in the β2-strand of NtMYC2a^{D128P} (yellow) dramatically lost extended β-strand confirmation to unidentified structure (none) compared to the other three models, which remain mostly extended β2-strand. D. Position M193 in of α4 in TAD of NtMYC2a^{D128P} (yellow) also dramatically changed confirmation into 3_{10}-helix. E. Long-distance changes are imposed on position L163 in NtMYC2a^{D128P} and result in increases in bending and turning. *F. helix* α3 occludes the JID binding pocket where L163 of α3, M193 of α4, and W126 and P128 of β2 are indicated.

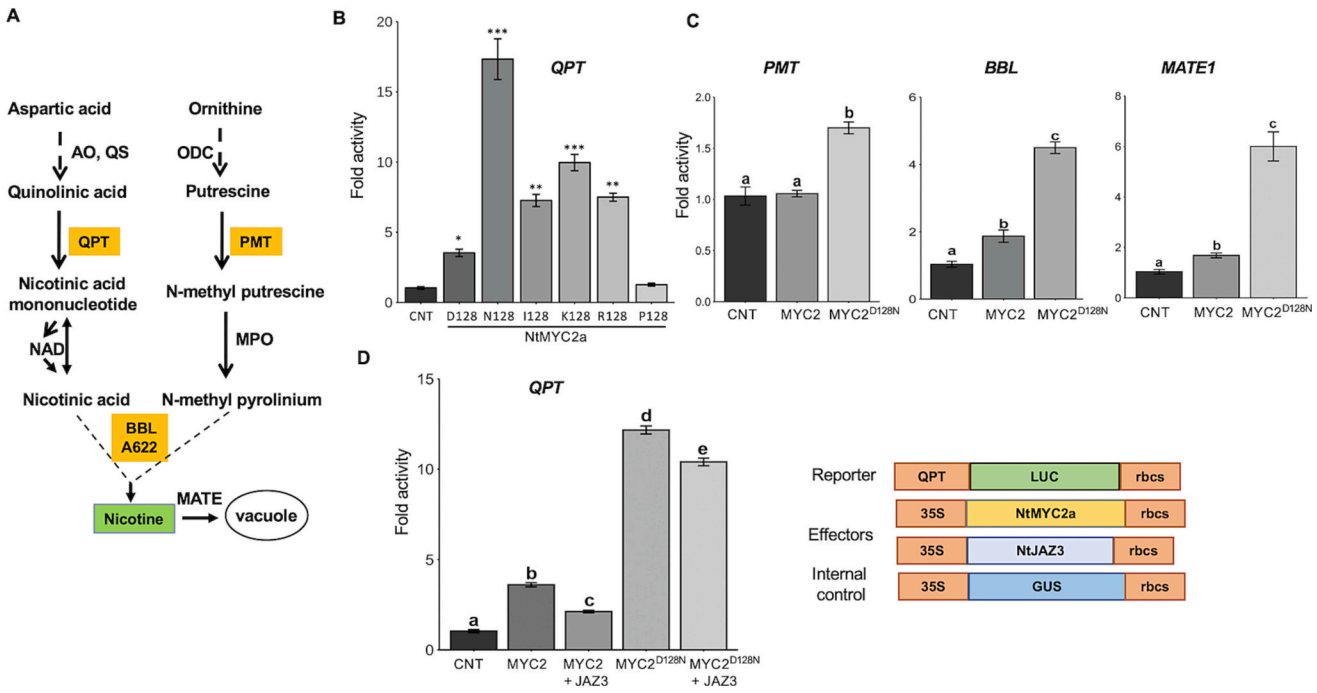

Fig. 5. Transactivation of the nicotine pathway gene promoters by NtMYC2a^{D128N} in tobacco cells. A. Schematic diagram of the nicotine biosynthetic pathway in tobacco. A622, isoflavone reductase-like protein; ADC, arginine decarboxylase; AO, aspartate oxidase; BBL, berberine bridge enzyme-like; ODC, ornithine decarboxylase; MPO, *N*-methylputrescine oxidase; QPT, quinolinate phosphoribosyltransferase; QS, quinolinate synthase; PMT, putrescine *N*-methyltransferase. B. Transactivation of the *QPT* promoter by *NtMYC2a* and *NtMYC2a* mutants (NtMYC2a^{D128N}, NtMYC2a^{D128I}, NtMYC2a^{D128K}, NtMYC2a^{D128R}, and NtMYC2a^{D128P}) in tobacco cells. C. Transactivation of the *PMT*, *BBL* and *MATE1* promoters by NtMYC2a and NtMYC2a^{D128N} in tobacco cells. The *LUC* reporter driven by the promoters were electroporated into tobacco protoplasts, alone or in combination, with an effector *CaMV*35S-*NtMYC2a* (MYC2) or *NtMYC2a* mutants. A *CaMV*35S-*GUS* served as an internal control. GUS activity was used to normalize the LUC activity. Data of three independent experiments with means±SD are presented. Student's *t*-test was used for calculating statistical significance: *, $P < 0.05$; **, $P < 0.01$; ***, $P < 0.001$ D. Transactivation of the *QPT* promoter by NtMYC2a, NtMYC2a^{D128N} and NtJAZ3 in tobacco cells. The *LUC* reporter driven by the *QPT* promoter was electroporated into tobacco protoplasts alone or in combination with an effector (CaMV35S-NtMYC2a, NtMYC2a^{D128N}, NtJAZ3). Schematic diagrams of reporter, effectors and internal control are shown in the bottom right. Data presented are means±SD of three independent experiments. Different letters denote statistical differences as assessed by one-way ANOVA and Tukey HSD test, $P < 0.05$.

Arabidopsis MYC2 and MYC3 enhances the activity of both TFs on expression of target genes [14,64]. Although possible causes have been proposed [14], a comprehensive analysis and experimental support were lacking. The previous work only has tested one amino acid substitution, thus lacking the structural insights to the impact by the conserved D residue. More importantly, the impacts on interaction of the D-to-N mutant with MED25 had not been studied as the MYC2-MED25 interaction is a more recent discovery. In this work, using tobacco as a model, we demonstrated that mutation to D128 in the NtMYC2 JID-TAD alters its interaction with JAZ proteins and NtMED25, leading to altered transactivation of the nicotine pathway promoters, and overexpression of *NtMYC2a*^{D128N} increased nicotine accumulation in tobacco hairy roots. We also gained insights into the effects of mutations at D128 to the structural stability of JID.

The structural and regulatory genes in the nicotine biosynthetic pathway are induced by JA. JAZ3 and JAZ8 play crucial roles in JA signaling in Arabidopsis [9,52]. Similar to the nicotine pathway genes, all four tobacco JAZs are highly expressed in roots and respond to JA treatment (Fig. 1). The JID-TAD, essential for interaction with JAZ, is well conserved in tobacco MYC2s (Fig. S1), and the amino acid residues in the Jas domain critical for interaction with NtMYC2 are present in tobacco JAZs (Fig. 2B). MED25, a key integrator of JA signaling, interacts with MYC2 to promote the assembly of the preinitiation complex for transcription initiation [15]. We demonstrated that NtMED25 interacts with NtMYC2a (Fig. 3). Our findings further confirm the conserved nature of the JA signaling pathway in plants.

Structural analysis of Arabidopsis MYC3-JAZ9 interaction reveals that the conserved aspartic acid (D94) in MYC3 JID forms charge interaction with the arginine 229 (R229) in the Jas domain of JAZ9, suggesting the importance of this residue in MYC-JAZ interaction [13]. Mutations D94N in MYC3 and D105N in MYC2 abolished interaction with many JAZ proteins in Arabidopsis [14]. The saturation mutagenesis systematically substituted the wildtype amino acid residue (D128) of NtMYC2a and allowed us to examine a large number of variants potentially with altered functions. NtMYC2a^{D128N} lost the interaction with NtJAZ2 and NtJAZ3, but not NtJAZ1 and NtJAZ8 (Fig. 2). NtMYC2a^{D128N} is thus partially desensitized to sequestration by NtJAZ proteins as it lost the ability to interact with two NtJAZs. The D128N mutation, however, does not affect the interaction of NtMYC2a^{D128N} with NtMED25 (Fig. 3). Similarly, in *C. roseus*, D126N mutation in CrMYC2 abolished interaction with CrJAZ2, CrJAZ3 and CrJAZ8, but not CrJAZ1 (Fig. S8), highlighting the importance of this aspartic acid in the JID of MYC2 for interaction with JAZ proteins in other plant species. In addition to the Jas domain, a CMID (cryptic MYC-interaction domain) has been identified at the amino termini of several Arabidopsis JAZ proteins [11,12]. The amino acid residues in CMID are also conserved in tobacco and *C. roseus* JAZ1 (Fig. S2). In both tobacco and *C. roseus*, NtJAZ1 and CrJAZ1 interact with the MYC2 and the MYC2 mutants possibly through the CMID (Fig. 2 and Fig. S8). Substitution of D128 in NtMYC2a with 19 other amino acids yielded a wide range of responses (Table 1). Based on cell growth on quadruple selection, it appears that the glycine (G), histidine (H), and tyrosine (Y) substitutions weakened, while the lysine (K), isoleucine (I), arginine (R), and proline (P) substitutions at D128 completely abolished the interaction of NtMYC2a with tobacco JAZ proteins (Table 1).

Homology modeling revealed that compared to the NtMYC2a (D128), the β2-strand appeared to be further stabilized by the D128N substitution (Fig. 4). D128N enables the formation of a consistently

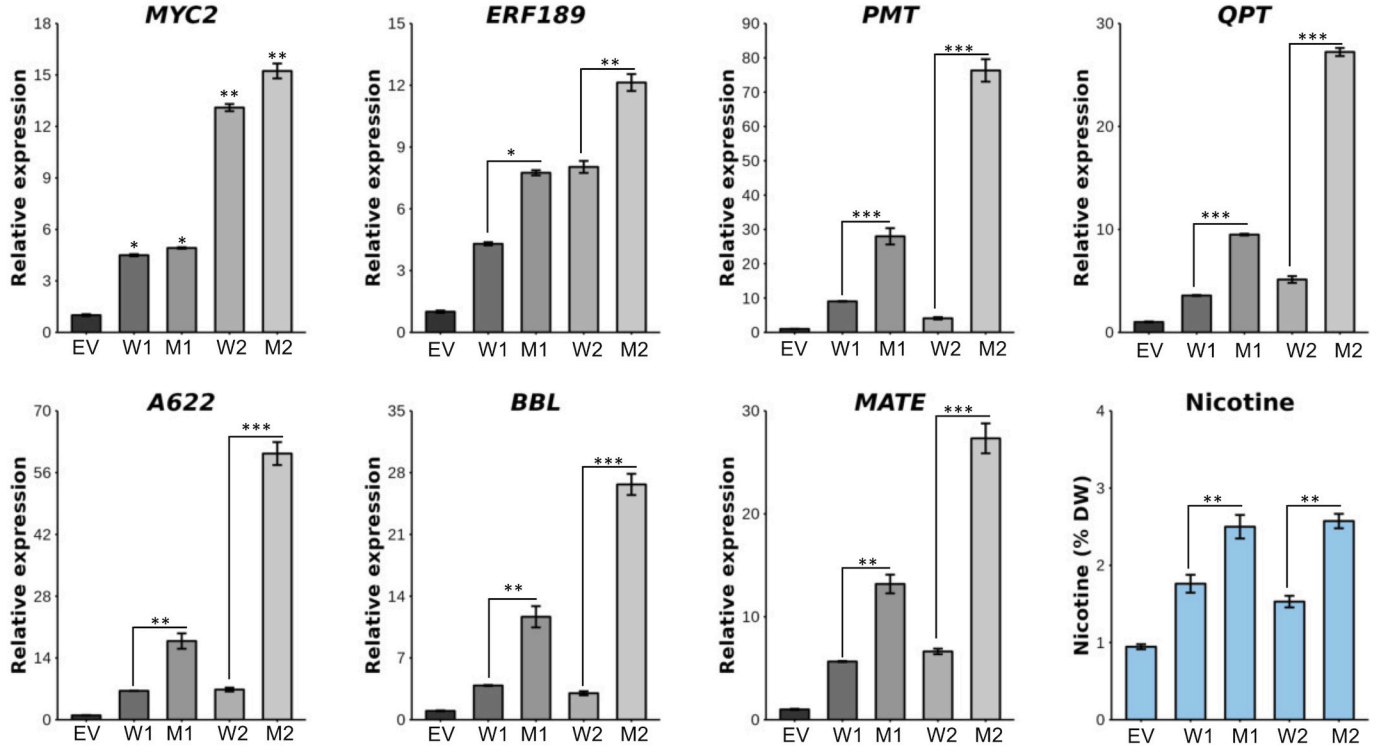

Fig. 6. NtMYC2a^{D128N} overexpression significantly activates the expression of nicotine pathway genes and increases nicotine accumulation in tobacco hairy roots. Expression of nicotine pathway genes in hairy roots transformed with empty vector (EV), NtMYC2a (W1 and W2), or NtMYC2a^{D128N} (M1 and M2) was measured using RT-qPCR. Tobacco *EF1α* was used as an internal control. Data represent mean ± SD of three biological samples. Nicotine contents in transgenic hairy roots (EV, NtMYC2a and NtMYC2a^{D128N}) were measured using GC-FID and presented as percentage dry weight (DW). Data presented are mean ± SD of three biological replicates. W1 and W2, NtMYC2a line 1 and line 2; M1 and M2, NtMYC2a^{D128N} mutant line 1 and line 2. Student's *t*-test was used for calculating statistical significance: *, $P < 0.05$; **, $P < 0.01$; ***, $P < 0.001$.

extended β2-strand with little variations (Fig. 4A-C). The stabilization of the β2-strand seemingly also stabilizes the JID binding pocket which comprises β2, α3 and α4 (Fig. 4F). Electrostatic charge interactions are likely critical to keeping the JID binding pocket open and available to JAZ protein entry and binding (Fig. S9). The surface of the JID binding pocket, especially the α3 helix, is rich in hydrophobic amino acids. The simulated substitution of hydrophobic residues, such as isoleucine and proline, for the acidic aspartic acid in the β2-strand revealed the creation of a potential hydrophobic interaction network between the β2 strand and the α3 helix that may be strong enough to prohibit entry of JAZ proteins for binding, and in the case of proline, possibly prohibit the entry of NtMED25. The strength of this hydrophobic interaction network was observable in our molecular dynamic simulations by showing the formation of a break (turn/bend) in the α3 helix around L163 (Fig. 4E and F) and movement of the C-terminal end of α3 helix to occupy the JID binding pocket.

MED25 interacts with MYC2 and MYC3 through JID-TAD. It has been proposed that the Jas motif JAZ and the ACID domain of the Arabidopsis MED25 bind to a shared surface of MYC3 [13]. We were thus intrigued to evaluate the interaction of NtMYC2a mutants with NtMED25. All 19 mutants, except NtMYC2a^{D128P}, interact with NtMED25 (Fig. 3; Table 2). The D128P substitution has a drastic effect on the interaction of NtMYC2a with NtMED25. Prior to this work, the structure-function relationship underlying the NtMYC2a-NtMED25 was not well examined. We performed structural modeling to gain insights into the effect of the proline substitution on NtMYC2a-NtMED25 interaction. The degree of instability found in the JID binding pocket of NtMYC2a^{D128P} by molecular dynamics simulations also suggests that JID is the location and surface for NtMED25 binding and interaction. It suggests that the instability of the β2-strand in NtMYC2a^{D128P} is too great to allow for stable NtMED25 binding interaction as seen with various JAZ proteins (Figs. 3, 4A and B). Considering no difference was seen between any other residues besides proline (Table 2), it is most likely that the instability created by a proline substitution is greater than the ability to form a stable NtMYC2-NtMED25 interaction. The molecular dynamics, together with reduced changes in secondary structure and the protein-protein interaction data, suggest that the D128N substitution has an overall stabilizing effect on the binding pocket. The residue M193 (TAD; α4) (Fig. 4D) showed an approximately threefold increase in the 3_{10}-helix confirmation in time spent compared to the other three models (Fig. 4E), suggesting that the D128P mutation may be pushing the C-terminal end of the α4 helix into a transitional structure and destabilizing the helix. Additionally, in the apo crystal structures of AtMYC3, N-terminal α-helix (α1-α1') occupies this same location in the absence of a JAZ interaction partner [13]. NtMYC2^{D128P}, located on the same JID-binding surface, shows hallmarks of disrupted MED25 interaction, again suggesting that this surface interacts with NtMED25. In the case of the predicted NtMED25 model, the two α-helices are separated by a bend aligned with the primary and secondary structures of the MED25^{CMIDM} region (Fig. S9), as mentioned by [65].

The transactivation activities of NtMYC2a and NtMYC2a^{D128N} on the nicotine pathway gene promoters were evaluated in tobacco cells. The transactivation activity of NtMYC2a^{D128N} was significantly higher on all tested promoters compared to NtMYC2a (Fig. 5B-C). This is unlike what has been observed in Arabidopsis, where both MYC2 and MYC2^{D105N} transactivate the *LOX3* promoter to a similar extent. Co-expression of *AtJAZ* genes completely attenuated the activity of AtMYC2 on the *LOX3* promoter, whereas that of *MYC2^{D105N}* is reduced, although remaining active, in the presence of JAZ [14]. In tobacco, co-expression of *NtJAZ3* reduced the activity of both NtMYC2a and NtMYC2a^{D128N} on the *QPT* promoter; however, the reduction was significantly higher for NtMYC2a compared to NtMYC2a^{D128N} (Fig. 5D). The reduced activity of

NtMYC2a^{D128N} is likely due to the presence of other NtJAZ proteins in tobacco cells that interact with the mutant. Overexpression of *NtMYC2a*^{D128N} significantly upregulated the nicotine pathway genes and increased nicotine accumulation in tobacco hairy roots compared to *NtMYC2a* (Fig. 6). Taken together, these findings suggest that the increased transactivation capacity and partial desensitization of NtMYC2 from NtJAZ-mediated repression, even in the absence of JA, boost gene expression and metabolic outcomes. Consequently, the same binding pocket in the desensitized MYC2 mutant is more readily accepting the coactivators, such as NtMED25. In Arabidopsis, JAZ and MED25 have been proposed to dock the same binding surface in MYC3 [13], and our homology modeling also supports this conclusion (Fig. S9).

We summarized our findings in a simple hypothetical model (Fig. 7). NtMYC2a co-regulates nicotine pathway genes with the AP2/ERFs (ERF) and interacts with NtJAZ proteins to form a repressor complex with NtTPL through the adapter protein NtNINJA (Fig. 7; Fig. S10). NtMED25 competes with NtJAZ proteins for the same binding interface in NtMYC2a. In *NtMYC2a*-overexpressing hairy roots, the abundance of the repressor complex is presumably more prevalent than the NtMYC2a-NtMED25 activator complex, resulting in moderate expression of the pathway genes. In plant cells expressing the partially desensitized *NtMYC2a*^{D128N}, the abundance of the NtMYC2a^{D128N}-MED25 activator complex will likely be significantly higher than the NtMYC2-NtJAZ repressor complex. This leads to higher expression of the pathway genes and increased metabolic outcomes. As *NtMYC2a*^{D128P} does not interact with NtJAZ or NtMED25, it is unable to activate the pathway genes. In Arabidopsis, MYC2, MYC3 and MYC4 interact with a group of R2R3MYBs to regulate GSL biosynthesis [66]. Whether MYC2s in tobacco or other plants interact MYBs to regulate various metabolic pathways is not known. Nonetheless, the partial de-repression of NtMYC2a (NtMYC2a^{D128N}) improves the interaction with NtMED25, and possibly other coactivators, to boost nicotine biosynthesis.

5. Conclusion

Our work is novel in several aspects. First, we provided a comprehensive survey on the role of D128 of NtMYC2a in affecting JAZ-mediated repression. Second, for the first time we associated D128 with the interaction of NtMYC2a with NtMED25. Furthermore, we gained structural insights to the N and P substitutions. While both variants are desensitized to JAZ repression, the ability of NtMYC2a^{D128N} and the inability of NtMYC2a^{D128P} to interact with NtMED25 determine the transactivation capacity. Additionally, we demonstrated that NtMYC2a^{D128N} significantly activated the promoters of nicotine pathway gene and increased nicotine accumulation in transgenic hairy roots. As MYC2 is a regulator of diverse specialized metabolites and the aspartic acid (D) in JID is well conserved across species, the aspartic acid mutants can be explored for manipulating metabolic pathways to boost the production of bioactive compounds in other plants. Much effort in engineering TFs has been directed to improving DNA-binding or transactivation activity. Our approach of desensitizing a TF from repression is shown here to be highly effective for engineering plant metabolic pathways. MYC2 functions by physically interacting with the coactivator MED25 [67]. Therefore, it is important to note that only desensitization of MYC2 to JAZ-mediated repression is insufficient for pathway upregulation. NtMYC2a^{D128N} is effective because it is partially desensitized to the repression while maintaining strong interaction with

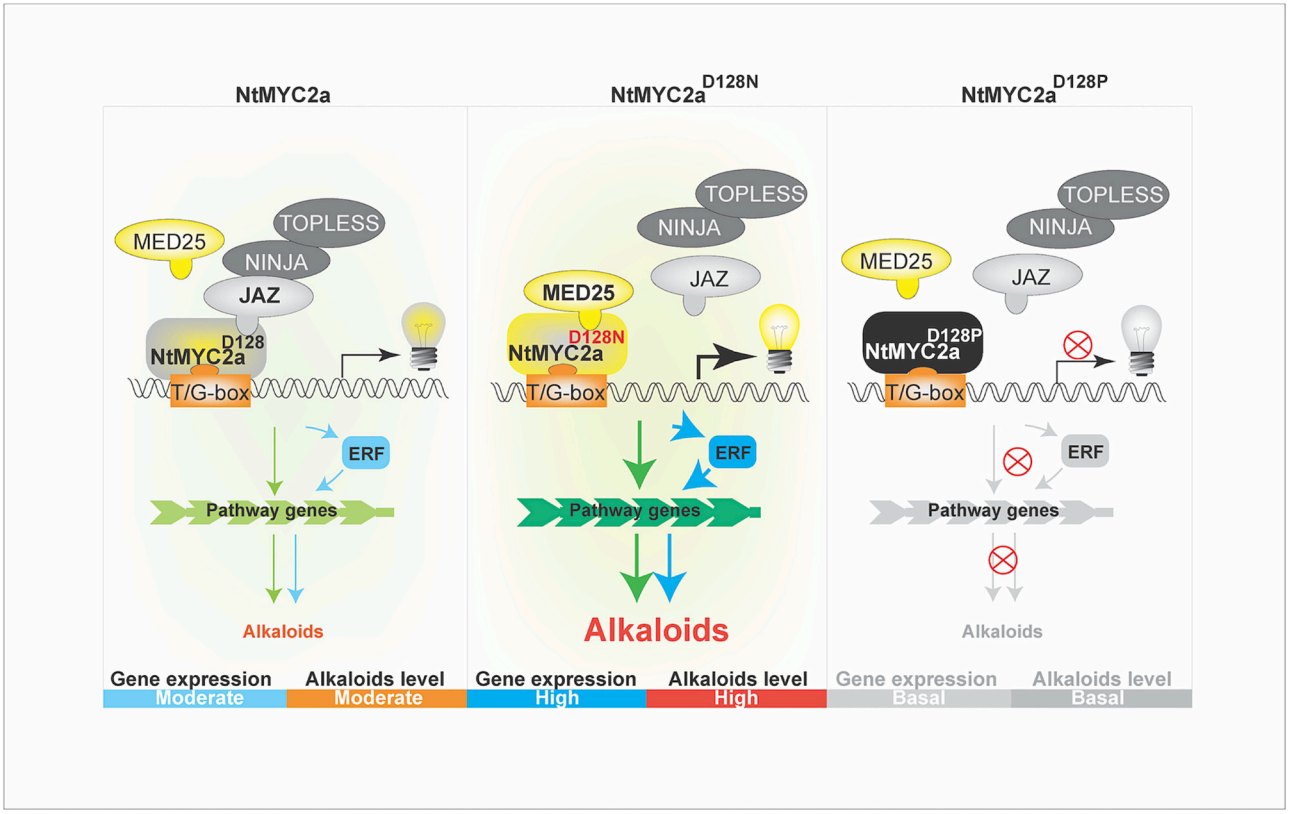

Fig. 7. A model illustrating the regulation of nicotine pathway by *NtMYC2a*, *NtMYC2a*^{D128N}, and *NtMYC2a*^{D128P}. NtMYC2a interacts with NtJAZ proteins that form a repressor complex with NtTPL and NtNINJA. NtMED25 competes with NtJAZ proteins for the same binding interface in NtMYC2a. In *NtMYC2a*-overexpressing hairy roots, the abundance of the repressor complex is presumably more prevalent than the MYC2-MED25 activator complex resulting in moderate expression of the pathway genes. In plant cells expressing the partially desensitized *NtMYC2a*^{D128N}, the abundance of the NtMYC2a^{D128N}-MED25 activator complex will likely be significantly higher than the NtMYC2-NtJAZ repressor complex. This leads to higher expression of the pathway genes and increased metabolic outcome. As *NtMYC2a*^{D128P} does not interact with NtJAZ or NtMED25, it is unable to activate the pathway genes.

NtMED25. The additional D128 mutants generated in this study will allow us to further examine the effects of this residue in the JID binding pocket, leading to altered metabolic outcomes.

Ethics requirements

This work does not involve human or animal subjects.

CRediT authorship contribution statement

S.P., and L.Y. conceived and supervised the project. X.H, S.K.S., YL. L., Q.Y., B.P., X.W. and R.L., X.L. performed the experiments. J.R.W. performed structural modeling. X.H, S.K.S., Y.L., Q.Y., X.S. B.W. Y.L, and W.M. analyzed data. S.P., J.R.W., S.K.S. and L.Y. wrote the manuscript.

Declaration of competing interest

The authors declare no conflicts of interest.

Data availability

Data will be made available on request.

Acknowledgements

This work is supported partially by the Harold R. Burton Endowed Professorship to L.Y., and by the grants 2018530000241001 and 2022530000241012 from the Yunnan Tobacco Company, the National Key Research and Development Program of China (2019YFC1711100), the Kentucky Tobacco Research and Development Center (KTRDC), The Shandong Province Modern Agricultural Technology System (SDAIT-25-02), The China Tobacco Shandong Industrial Corporation Major Project (202102004), The Shandong Tobacco Company Science and Technology Project (KN294, KN291, KN293, KN287), The Shandong Weifang Tobacco Company Science and Technology Project (2021-57), and The Shandong Rizhao Tobacco Company Science and Technology Project (2022-003). We would like to thank Huihua Ji for assistance in measuring nicotine contents in the hairy roots.

Appendix A. Supplementary data

Supplementary data to this article can be found online at https://doi.org/10.1016/j.ijbiomac.2023.126472.

References

[1] A. Feller, et al., Evolutionary and comparative analysis of MYB and bHLH plant transcription factors, Plant J. 66 (2011) 94–116, https://doi.org/10.1111/j.1365-313X.2010.04459.x.
[2] M.A. Heim, et al., The basic helix-loop-helix transcription factor family in plants: a genome-wide study of protein structure and functional diversity, Mol. Biol. Evol. 20 (2003) 735–747, https://doi.org/10.1093/molbev/msg088.
[3] K. Kazan, J.M. Manners, MYC2: the master in action, Mol. Plant 6 (2013) 686–703, https://doi.org/10.1093/mp/sss128.
[4] A. Chini, et al., The JAZ family of repressors is the missing link in jasmonate signalling, Nature 448 (2007) 666–671, https://doi.org/10.1038/nature06006.
[5] P. Fernandez-Calvo, et al., The Arabidopsis bHLH transcription factors MYC3 and MYC4 are targets of JAZ repressors and act additively with MYC2 in the activation of jasmonate responses, Plant Cell 23 (2011) 701–715, https://doi.org/10.1105/tpc.110.080788.
[6] T. Qi, et al., Regulation of Jasmonate-mediated stamen development and seed production by a bHLH-MYB complex in arabidopsis, Plant Cell 27 (2015) 1620–1633, https://doi.org/10.1105/tpc.15.00116.
[7] L. Pauwels, et al., NINJA connects the co-repressor TOPLESS to jasmonate signalling, Nature 464 (2010) 788–791, https://doi.org/10.1038/nature08854.
[8] L. Pauwels, A. Goossens, The JAZ proteins: a crucial interface in the jasmonate signaling cascade, Plant Cell 23 (2011) 3089–3100, https://doi.org/10.1105/tpc.111.089300.
[9] B. Thines, et al., JAZ repressor proteins are targets of the SCF(COI1) complex during jasmonate signalling, Nature 448 (2007) 661–665, https://doi.org/10.1038/nature05960.
[10] H.S. Chung, G.A. Howe, A critical role for the TIFY motif in repression of jasmonate signaling by a stabilized splice variant of the JASMONATE ZIM-domain protein JAZ10 in Arabidopsis, Plant Cell 21 (2009) 131–145, https://doi.org/10.1105/tpc.108.064097.
[11] F. Zhang, et al., Structural insights into alternative splicing-mediated desensitization of jasmonate signaling, Proc. Natl. Acad. Sci. U. S. A. 114 (2017) 1720–1725, https://doi.org/10.1073/pnas.1616938114.
[12] J.E. Moreno, et al., Negative feedback control of jasmonate signaling by an alternative splice variant of JAZ10, Plant Physiol. 162 (2013) 1006–1017, https://doi.org/10.1104/pp.113.218164.
[13] F. Zhang, et al., Structural basis of JAZ repression of MYC transcription factors in jasmonate signalling, Nature 525 (2015) 269–273, https://doi.org/10.1038/nature14661.
[14] J. Goossens, et al., Change of a conserved amino acid in the MYC2 and MYC3 transcription factors leads to release of JAZ repression and increased activity, New Phytol. 206 (2015) 1229–1237, https://doi.org/10.1111/nph.13398.
[15] Q. Zhai, et al., Mediator subunit MED25: at the nexus of jasmonate signaling, Curr. Opin. Plant Biol. 57 (2020) 78–86, https://doi.org/10.1016/j.pbi.2020.06.006.
[16] Q. Zhai, C. Li, The plant mediator complex and its role in jasmonate signaling, J. Exp. Bot. 70 (2019) 3415–3424, https://doi.org/10.1093/jxb/erz233.
[17] H. Huang, et al., Jasmonate action in plant growth and development, J. Exp. Bot. 68 (2017) 1349–1359, https://doi.org/10.1093/jxb/erw495.
[18] L. Zhang, et al., Jasmonate signaling and manipulation by pathogens and insects, J. Exp. Bot. 68 (2017) 1371–1385, https://doi.org/10.1093/jxb/erw478.
[19] Q. Shen, et al., The jasmonate-responsive AaMYC2 transcription factor positively regulates artemisinin biosynthesis in Artemisia annua, New Phytol. 210 (2016) 1269–1281, https://doi.org/10.1111/nph.13874.
[20] S.K. Lenka, et al., Jasmonate-responsive expression of paclitaxel biosynthesis genes in Taxus cuspidata cultured cells is negatively regulated by the bHLH transcription factors TcJAMYC1, TcJAMYC2, and TcJAMYC4, Front. Plant Sci. 6 (2015) 115, https://doi.org/10.3389/fpls.2015.00115.
[21] B. Patra, et al., A network of jasmonate-responsive bHLH factors modulate monoterpenoid indole alkaloid biosynthesis in Catharanthus roseus, New Phytol. 217 (2018) 1566–1581, https://doi.org/10.1111/nph.14910.
[22] X. Sui, et al., Cross-family transcription factor interaction between MYC2 and GBFs modulates terpenoid indole alkaloid biosynthesis, J. Exp. Bot. 69 (2018) 4267–4281, https://doi.org/10.1093/jxb/ery229.
[23] H. Zhang, et al., The basic helix-loop-helix transcription factor CrMYC2 controls the jasmonate-responsive expression of the ORCA genes that regulate alkaloid biosynthesis in Catharanthus roseus, Plant J. 67 (2011) 61–71, https://doi.org/10.1111/j.1365-313X.2011.04575.x.
[24] R.E. Dewey, J. Xie, Molecular genetics of alkaloid biosynthesis in Nicotiana tabacum, Phytochem 94 (2013) 10–27, https://doi.org/10.1016/j.phytochem.2013.06.002.
[25] T. Shoji, T. Hashimoto, Tobacco MYC2 regulates jasmonate-inducible nicotine biosynthesis genes directly and by way of the NIC2-locus ERF genes, Plant Cell Physiol. 52 (2011) 1117–1130, https://doi.org/10.1093/pcp/pcr063.
[26] B. Wang, et al., Genetic factors for enhancement of nicotine levels in cultivated tobacco, Sci. Rep. 5 (2015) 17360, https://doi.org/10.1038/srep17360.
[27] L. Yuan, Clustered ERF transcription factors: not all created equal, Plant Cell Physiol. 61 (2020) 1025–1027, https://doi.org/10.1093/pcp/pcaa067.
[28] H.B. Zhang, et al., Tobacco transcription factors NtMYC2a and NtMYC2b form nuclear complexes with the NtJAZ1 repressor and regulate multiple jasmonate-inducible steps in nicotine biosynthesis, Mol. Plant 5 (2012) 73–84, https://doi.org/10.1093/mp/ssr056.
[29] C. Yang, et al., Exploring the metabolic basis of growth/defense trade-offs in complex environments with Nicotiana attenuata plants cosilenced in NaMYC2a/b expression, New Phytol. 238 (2023) 349–366, https://doi.org/10.1111/nph.18732.
[30] Q. Qin, et al., NIC1 cloning and gene editing generates low-nicotine tobacco plants, Plant Biotechnol. J. 19 (2021) 2150–2152, https://doi.org/10.1111/pbi.13694.
[31] T. Shoji, The recruitment model of metabolic evolution: Jasmonate-responsive transcription factors and a conceptual model for the evolution of metabolic pathways, Front. Plant Sci. 10 (2019) 560, https://doi.org/10.3389/fpls.2019.00560.
[32] T. Shoji, et al., Jasmonate-induced nicotine formation in tobacco is mediated by tobacco COI1 and JAZ genes, Plant Cell Physiol. 49 (2008) 1003–1012, https://doi.org/10.1093/pcp/pcn077.
[33] X. Liu, et al., Protein phosphatase NtPP2C2b and MAP kinase NtMPK4 act in concert to modulate nicotine biosynthesis, J. Exp. Bot. 72 (2021) 1661–1676, https://doi.org/10.1093/jxb/eraa568.
[34] P. Paul, et al., Mutually regulated AP2/ERF gene clusters modulate biosynthesis of specialized metabolites in plants, Plant Physiol. 182 (2020) 840–856, https://doi.org/10.1104/pp.19.00772.
[35] N. Sierro, et al., The tobacco genome sequence and its comparison with those of tomato and potato, Nat. Commun. 5 (2014) 3833, https://doi.org/10.1038/ncomms4833.
[36] X. Sui, et al., Unravel the mystery of NIC1-locus on nicotine biosynthesis regulation in tobacco, BioRxiv. (2020), https://doi.org/10.1101/2020.07.04.187922.
[37] R. Schmieder, R. Edwards, Quality control and preprocessing of metagenomic datasets, Bioinformatics 27 (2011) 863–864, https://doi.org/10.1093/bioinformatics/btr026.
[38] B. Langmead, S.L. Salzberg, Fast gapped-read alignment with Bowtie 2, Nat. Met. 9 (2012) 357–359, https://doi.org/10.1038/nmeth.1923.

[39] N. Fernandez-Pozo, et al., The Sol Genomics Network (SGN)—from genotype to phenotype to breeding, Nucleic Acids Res. 43 (2015) D1036–D1041, https://doi.org/10.1093/nar/gku1195.
[40] Z. Gu, et al., Complex heatmaps reveal patterns and correlations in multidimensional genomic data, Bioinformatics 32 (2016) 2847–2849, https://doi.org/10.1093/bioinformatics/btw313.
[41] S. Pattanaik, et al., Site-directed mutagenesis and saturation mutagenesis for the functional study of transcription factors involved in plant secondary metabolite biosynthesis, Met. Mol. Biol. 643 (2010) 47–57, https://doi.org/10.1007/978-1-60761-723-5_4.
[42] D.E. Riechers, M.P. Timko, Structure and expression of the gene family encoding putrescine N-methyltransferase in Nicotiana tabacum: new clues to the evolutionary origin of cultivated tobacco, Plant Mol. Biol. 41 (1999) 387–401, https://doi.org/10.1023/a:1006342018991.
[43] T. Shoji, T. Hashimoto, Recruitment of a duplicated primary metabolism gene into the nicotine biosynthesis regulon in tobacco, Plant J. 67 (2011) 949–959, https://doi.org/10.1111/j.1365-313X.2011.04647.x.
[44] T. Shoji, et al., Multidrug and toxic compound extrusion-type transporters implicated in vacuolar sequestration of nicotine in tobacco roots, Plant Physiol. 149 (2009) 708–718, https://doi.org/10.1104/pp.108.132811.
[45] D. Weigel, J. Glazebrook, Transformation of agrobacterium using the freeze-thaw method, CSH Protoc. 2006 (2006), https://doi.org/10.1101/pdb.prot4666.
[46] K.J. Livak, T.D. Schmittgen, Analysis of relative gene expression data using real-time quantitative PCR and the 2(-Delta Delta C(T)) method, Methods 25 (2001) 402–408, https://doi.org/10.1006/meth.2001.1262.
[47] T. Shoji, et al., Clustered transcription factor genes regulate nicotine biosynthesis in tobacco, Plant Cell 22 (2010) 3390–3409, https://doi.org/10.1105/tpc.110.078543.
[48] G. Studer, et al., ProMod3-a versatile homology modelling toolbox, PLoS Comput. Biol. 17 (2021), e1008667, https://doi.org/10.1371/journal.pcbi.1008667.
[49] D.A. Case, et al., Amber 2022, University of California, San Francisco, 2022.
[50] W. Kabsch, C. Sander, Dictionary of protein secondary structure: pattern recognition of hydrogen-bonded and geometrical features, Biopolymers 22 (1983) 2577–2637, https://doi.org/10.1002/bip.360221211.
[51] S.M. Mortuza, et al., Improving fragment-based ab initio protein structure assembly using low-accuracy contact-map predictions, Nat. Commun. 12 (2021) 5011, https://doi.org/10.1038/s41467-021-25316-w.
[52] C. Shyu, et al., JAZ8 lacks a canonical degron and has an EAR motif that mediates transcriptional repression of jasmonate responses in Arabidopsis, Plant Cell 24 (2012) 536–550, https://doi.org/10.1105/tpc.111.093005.
[53] B. Patra, et al., Transcriptional regulation of secondary metabolite biosynthesis in plants, Biochim. Biophys. Acta 1829 (2013) 1236–1247, https://doi.org/10.1016/j.bbagrm.2013.09.006.
[54] M. Kajikawa, et al., Genomic insights into the evolution of the nicotine biosynthesis pathway in tobacco, Plant Physiol. 174 (2017) 999–1011, https://doi.org/10.1104/pp.17.00070.
[55] P. Paul, et al., A differentially regulated AP2/ERF transcription factor gene cluster acts downstream of a MAP kinase cascade to modulate terpenoid indole alkaloid biosynthesis in Catharanthus roseus, New Phytol. 213 (2017) 1107–1123, https://doi.org/10.1111/nph.14252.
[56] S.K. Singh, et al., Revisiting the ORCA gene cluster that regulates terpenoid indole alkaloid biosynthesis in Catharanthus roseus, Plant Sci. 293 (2020), 110408, https://doi.org/10.1016/j.plantsci.2020.110408.
[57] P.D. Cardenas, et al., GAME9 regulates the biosynthesis of steroidal alkaloids and upstream isoprenoids in the plant mevalonate pathway, Nat. Commun. 7 (2016) 10654, https://doi.org/10.1038/ncomms10654.
[58] C. Thagun, et al., Jasmonate-responsive ERF transcription factors regulate steroidal glycoalkaloid biosynthesis in tomato, Plant Cell Physiol. 57 (2016) 961–975, https://doi.org/10.1093/pcp/pcw067.
[59] M. Nakayasu, et al., JRE4 is a master transcriptional regulator of defense-related steroidal glycoalkaloids in tomato, Plant J. 94 (2018) 975–990, https://doi.org/10.1111/tpj.13911.
[60] S. Pattanaik, et al., Directed evolution of plant basic helix-loop-helix transcription factors for the improvement of transactivational properties, Biochim. Biophys. Acta 1759 (2006) 308–318, https://doi.org/10.1016/j.bbaexp.2006.04.009.
[61] Z.Z. Gong, et al., A constitutively expressed Myc-like gene involved in anthocyanin biosynthesis from Perilla frutescens: molecular characterization, heterologous expression in transgenic plants and transactivation in yeast cells, Plant Mol. Biol. 41 (1999) 33–44, https://doi.org/10.1023/a:1006237529040.
[62] J. Goodrich, et al., A common gene regulates pigmentation pattern in diverse plant species, Cell 68 (1992) 955–964, https://doi.org/10.1016/0092-8674(92)90038-e.
[63] S. Pattanaik, et al., The interaction domains of the plant Myc-like bHLH transcription factors can regulate the transactivation strength, Planta 227 (2008) 707–715, https://doi.org/10.1007/s00425-007-0676-y.
[64] G.A. Smolen, et al., Dominant alleles of the basic helix-loop-helix transcription factor ATR2 activate stress-responsive genes in Arabidopsis, Genetics 161 (2002) 1235–1246.
[65] Y. Takaoka, et al., Protein-protein interactions between jasmonate-related master regulator MYC and transcriptional mediator MED25 depend on a short binding domain, J. Biol. Chem. 298 (2022), 101504, https://doi.org/10.1016/j.jbc.2021.101504.
[66] F. Schweizer, et al., Arabidopsis basic helix-loop-helix transcription factors MYC2, MYC3, and MYC4 regulate glucosinolate biosynthesis, insect performance, and feeding behavior, Plant Cell 25 (2013) 3117–3132, https://doi.org/10.1105/tpc.113.115139.
[67] H. Wang, et al., MED25 connects enhancer-promoter looping and MYC2-dependent activation of jasmonate signalling, Nat. Plants 5 (2019) 616–625, https://doi.org/10.1038/s41477-019-0441-9.

FISCAL YEAR 2023 – 2024

FINANCIAL REPORT

April 1, 2024 – June 30, 2024

QUARTERLY REPORT

TOBACCO RESEARCH INCOME
INCOME COMPARISON

Fiscal Years	2017-2018	2018-2019	2019-2020	2020-2021	2021-2022	2022-2023	2023-2024
July	$ 2,459.48	$ 120,890.40	$ 141,864.01	$ 136,565.92	$ 102,816.87	$ 113,853.04	$ -
August	$ 292,266.42	$ 126,982.37	$ 145,789.42	$ 11,873.82	$ 148,863.59	$ 121,485.75	$ 235,814.07
September	$ 139,414.92	$ 178,553.92	$ 132,169.60	$ 261,157.23	$ 138,395.19	$ 143,503.64	$ 116,834.55
1st QUARTER	**$ 434,140.82**	**$ 426,426.69**	**$ 419,823.03**	**$ 409,596.97**	**$ 390,075.65**	**$ 378,842.43**	**$ 352,648.62**
October	$ 126,862.91	$ 97,793.84	$ 150,849.00	$ 141,682.93	$ 138,913.78	$ 131,512.77	$ 84,290.07
November	$ 123,267.74	$ 128,963.50	$ 117,280.34	$ 135,157.14	$ 101,844.54	$ 101,050.68	$ 132,736.05
December	$ 135,314.04	$ 175,277.00	$ 151,323.23	$ 159,616.92	$ 138,232.14	$ 113,515.64	$ 81,648.61
2nd QUARTER	**$ 385,444.69**	**$ 402,034.34**	**$ 419,452.57**	**$ 436,456.99**	**$ 378,990.46**	**$ 346,079.09**	**$ 298,674.73**
January	$ 127,719.90	$ 564,217.88	$ 120,247.87	$ 93,056.96	$ 116,044.01	$ 111,657.62	$ 101,501.91
February	$ 114,047.53	$ 141,118.46	$ 114,095.14	$ 125,797.09	$ 89,271.71	$ 78,955.86	$ 77,922.09
March	$ 159,645.83	$ 122,472.86	$ 403,962.17	$ 143,903.75	$ 140,521.53	$ 119,175.49	$ 105,636.69
3rd QUARTER	**$ 401,413.26**	**$ 827,809.20**	**$ 638,305.18**	**$ 362,757.80**	**$ 345,837.25**	**$ 309,788.97**	**$ 285,060.69**
April	$ 65,036.15	$ 146,789.57	$ 117,862.64	$ 144,970.47	$ 127,449.97	$ 79,639.90	$ 119,161.48
May	$ 209,087.27	$ 63,797.02	$ 141,525.18	$ 100,238.76	$ 148,769.94	$ 120,890.24	$ 88,889.28
June	$ 168,621.20	$ 250,352.13	$ 138,849.18	$ 211,130.06	$ 121,204.33	$ 133,854.96	$ 154,407.96
4th QUARTER	**$ 442,744.62**	**$ 460,938.72**	**$ 398,237.00**	**$ 456,339.29**	**$ 397,424.24**	**$ 334,385.10**	**$ 362,458.72**
TOTAL INCOME	**$ 1,663,743.39**	**$ 2,117,208.95**	**$ 1,875,817.78**	**$ 1,665,151.05**	**$ 1,512,327.60**	**$ 1,369,095.59**	**$ 1,298,842.76**

Funds Center		Commitment Item	Annual (Revised) Budget	Prior Balance	Current Month Actual	YTD Actual	Available Budget
1235410080	HOLDING ACCOUNT	Revenue	($2,200,000.00)	($1,298,842.76)		($1,298,842.76)	($901,157.24)
1235410080	Result	Total	($2,200,000.00)	($1,298,842.76)		($1,298,842.76)	($901,157.24)
1235410090	KENTUCKY TOBACCO RES	Operating Expens	$1,000.00	$472.74		$472.74	$527.26
1235410090	KENTUCKY TOBACCO RES	Recharges		$2.81		$2.81	($2.81)
1235410090	Result	Total	$1,000.00	$475.55		$475.55	$524.45
1235410100	ADMINISTRATION	Salaries	$288,500.00	$173,221.85		$173,221.85	$115,278.15
1235410100	ADMINISTRATION	Benefits		$45,958.47		$45,958.47	($45,958.47)
1235410100	ADMINISTRATION	Operating Expens		$15,213.16		$15,213.16	($15,213.16)
1235410100	ADMINISTRATION	Recharges		$25,233.29		$25,233.29	($25,233.29)
1235410100	Result	Total	$288,500.00	$259,626.77		$259,626.77	$28,873.23
1235410110	KTRDC PERSONNEL	Salaries	$1,169,300.00	$919,833.30		$919,833.30	$249,466.70
1235410110	KTRDC PERSONNEL	Benefits		$260,264.60		$260,264.60	($260,264.60)
1235410110	KTRDC PERSONNEL	Operating Expens		$372.00		$372.00	($372.00)
1235410110	KTRDC PERSONNEL	Recharges		$46,792.95		$46,792.95	($46,792.95)
1235410110	Result	Total	$1,169,300.00	$1,227,262.85		$1,227,262.85	($57,962.85)
1235410120	PUBLICATIONS & TRAVEL	Operating Expens	$40,000.00	$13,290.97		$13,290.97	$26,709.03
1235410120	PUBLICATIONS & TRAVEL	Recharges		$1,014.68		$1,014.68	($1,014.68)
1235410120	Result	Total	$40,000.00	$14,305.65		$14,305.65	$25,694.35
1235410130	BUILDING MAINTENANCE	Operating Expens	$70,000.00	$27,071.39		$27,071.39	$42,928.61
1235410130	BUILDING MAINTENANCE	Recharges		$10,041.13		$10,041.13	($10,041.13)
1235410130	Result	Total	$70,000.00	$37,112.52		$37,112.52	$32,887.48
1235410180	SHOP	Operating Expens	$2,000.00	$930.76		$930.76	$1,069.24
1235410180	SHOP	Recharges		$4.06		$4.06	($4.06)
1235410180	Result	Total	$2,000.00	$934.82		$934.82	$1,065.18

Funds Center		Commitment Item	Annual (Revised) Budget	Prior Balance	Current Month Actual	YTD Actual	Available Budget
1235410240	LABORATORY EQUIPMENT	Operating Expens	$44,200.00	$81,628.56		$81,628.56	($37,428.56)
1235410240	LABORATORY EQUIPMENT	Recharges		$714.31		$714.31	($714.31)
1235410240	Result	Total	$44,200.00	$82,342.87		$82,342.87	($38,142.87)
1235410250	UNALLOCATED RESERVE	Operating Expens	$90,000.00				$90,000.00
1235410250	Result	Total	$90,000.00				$90,000.00
1235410280	GENERAL LABORATORY	Operating Expens	$125,000.00	$34,983.82		$34,983.82	$90,016.18
1235410280	GENERAL LABORATORY	Recharges		$1,235.71		$1,235.71	($1,235.71)
1235410280	Result	Total	$125,000.00	$36,219.53		$36,219.53	$88,780.47
1235411040	DISCRETIONARY	Operating Expens	$10,000.00	$11,956.33		$11,956.33	($1,956.33)
1235411040	DISCRETIONARY	Recharges		$130.41		$130.41	($130.41)
1235411040	Result	Total	$10,000.00	$12,086.74		$12,086.74	($2,086.74)
1235411310	OUTREACH & COMMUNICA	Operating Expens	$30,000.00				$30,000.00
1235411310	Result	Total	$30,000.00				$30,000.00
1235411320	PLANT GENETIC ENGR	Salaries		$21,279.85		$21,279.85	($21,279.85)
1235411320	PLANT GENETIC ENGR	Benefits		$8,650.67		$8,650.67	($8,650.67)
1235411320	PLANT GENETIC ENGR	Operating Expens	$30,000.00				$30,000.00
1235411320	PLANT GENETIC ENGR	Recharges		$66.18		$66.18	($66.18)
1235411320	Result	Total	$30,000.00	$29,996.70		$29,996.70	$3.30
1235411340	GENETIC MANIPULATION	Salaries		$17,115.44		$17,115.44	($17,115.44)
1235411340	GENETIC MANIPULATION	Benefits		$5,307.07		$5,307.07	($5,307.07)
1235411340	GENETIC MANIPULATION	Operating Expens	$30,000.00	$4,107.50		$4,107.50	$25,892.50
1235411340	GENETIC MANIPULATION	Recharges		$3,467.05		$3,467.05	($3,467.05)
1235411340	Result	Total	$30,000.00	$29,997.06		$29,997.06	$2.94

Funds Center		Commitment Item	Annual (Revised) Budget	Prior Balance	Current Month Actual	YTD Actual	Available Budget
1235411360	PLANT BIOTECH METABO	Operating Expens	$30,000.00	$31,619.51		$31,619.51	($1,619.51)
1235411360	PLANT BIOTECH METABO	Recharges		$336.82		$336.82	($336.82)
1235411360	Result	Total	$30,000.00	$31,956.33		$31,956.33	($1,956.33)
1235411370	PLANT BIOTECH MOLECU	Operating Expens	$30,000.00	$25,530.42		$25,530.42	$4,469.58
1235411370	PLANT BIOTECH MOLECU	Recharges		$5,352.69		$5,352.69	($5,352.69)
1235411370	Result	Total	$30,000.00	$30,883.11		$30,883.11	($883.11)
1235411380	MOLECULAR GENETICS	Operating Expens	$30,000.00	$28,265.58		$28,265.58	$1,734.42
1235411380	MOLECULAR GENETICS	Recharges		$2,467.19		$2,467.19	($2,467.19)
1235411380	Result	Total	$30,000.00	$30,732.77		$30,732.77	($732.77)
1235411410	GREENHOUSE	Operating Expens	$30,000.00	$2,776.07		$2,776.07	$27,223.93
1235411410	GREENHOUSE	Recharges		$3,259.28		$3,259.28	($3,259.28)
1235411410	Result	Total	$30,000.00	$6,035.35		$6,035.35	$23,964.65
1235411430	PLANT ANALYTIC	Operating Expens	$30,000.00	$2,499.69		$2,499.69	$27,500.31
1235411430	PLANT ANALYTIC	Recharges		$29.12		$29.12	($29.12)
1235411430	Result	Total	$30,000.00	$2,528.81		$2,528.81	$27,471.19
1235411570	TOBACCO MOLECULAR	Operating Expens	$30,000.00	$7,387.94		$7,387.94	$22,612.06
1235411570	TOBACCO MOLECULAR	Recharges		$20,632.19		$20,632.19	($20,632.19)
1235411570	Result	Total	$30,000.00	$28,020.13		$28,020.13	$1,979.87
1235411640	GENE DISCOVERY	Salaries		$19,888.80		$19,888.80	($19,888.80)
1235411640	GENE DISCOVERY	Benefits		$7,163.26		$7,163.26	($7,163.26)
1235411640	GENE DISCOVERY	Operating Expens	$30,000.00	$0.00		$0.00	$30,000.00
1235411640	Result	Total	$30,000.00	$27,052.06		$27,052.06	$2,947.94

Funds Center		Commitment Item	Annual (Revised) Budget	Prior Balance	Current Month Actual	YTD Actual	Available Budget
1235412240	GREENHOUSE EVALUATIO	Salaries		$27,694.31		$27,694.31	($27,694.31)
1235412240	GREENHOUSE EVALUATIO	Benefits		$6,571.01		$6,571.01	($6,571.01)
1235412240	GREENHOUSE EVALUATIO	Operating Expens	$30,000.00				$30,000.00
1235412240	Result	Total	$30,000.00	$34,265.32		$34,265.32	($4,265.32)
1235412360	FLAVONOID - SMALLE	Salaries		$18,449.04		$18,449.04	($18,449.04)
1235412360	FLAVONOID - SMALLE	Benefits		$5,603.44		$5,603.44	($5,603.44)
1235412360	FLAVONOID - SMALLE	Operating Expens	$30,000.00	$640.03		$640.03	$29,359.97
1235412360	FLAVONOID - SMALLE	Recharges		$1.37		$1.37	($1.37)
1235412360	Result	Total	$30,000.00	$24,693.88		$24,693.88	$5,306.12

Kentucky Tobacco
Research & Development Center